NeuroImage: Clinical 3 (2013) 180–195

Contents lists available at ScienceDirect

NeuroImage: Clinical

journal homepage: www.elsevier.com/locate/ynicl

Effectiveness of regional DTI measures in distinguishing Alzheimer's disease, MCI, and normal aging ☆

Talia M. Nir [a], Neda Jahanshad [a], Julio E. Villalon-Reina [a], Arthur W. Toga [a], Clifford R. Jack [b], Michael W. Weiner [c], Paul M. Thompson [a,d,*] for the Alzheimer's Disease Neuroimaging Initiative (ADNI) [1]

[a] Imaging Genetics Center, Laboratory of Neuro Imaging, Department of Neurology, UCLA School of Medicine, Los Angeles, CA, USA
[b] Department of Radiology, Mayo Clinic and Foundation, Rochester, MN, USA
[c] Department of Radiology and Biomedical Imaging, UCSF School of Medicine, San Francisco, CA, USA
[d] Deptartment of Psychiatry, Semel Institute, UCLA School of Medicine, Los Angeles, CA, USA

ARTICLE INFO

Article history:
Received 3 April 2013
Received in revised form 3 July 2013
Accepted 21 July 2013
Available online xxxx

Keywords:
DTI
Alzheimer's disease
MCI
White matter
Clinical scores
Biomarkers

ABSTRACT

The Alzheimer's Disease Neuroimaging Initiative (ADNI) recently added diffusion tensor imaging (DTI), among several other new imaging modalities, in an effort to identify sensitive biomarkers of Alzheimer's disease (AD). While anatomical MRI is the main structural neuroimaging method used in most AD studies and clinical trials, DTI is sensitive to microscopic white matter (WM) changes not detectable with standard MRI, offering additional markers of neurodegeneration. Prior DTI studies of AD report lower fractional anisotropy (FA), and increased mean, axial, and radial diffusivity (MD, AxD, RD) throughout WM. Here we assessed which DTI measures may best identify differences among AD, mild cognitive impairment (MCI), and cognitively healthy elderly control (NC) groups, in region of interest (ROI) and voxel-based analyses of 155 ADNI participants (mean age: 73.5 ± 7.4; 90 M/65 F; 44 NC, 88 MCI, 23 AD). Both VBA and ROI analyses revealed widespread group differences in FA and all diffusivity measures. DTI maps were strongly correlated with widely-used clinical ratings (MMSE, CDR-sob, and ADAS-cog). When effect sizes were ranked, FA analyses were least sensitive for picking up group differences. Diffusivity measures could detect more subtle MCI differences, where FA could not. ROIs showing strongest group differentiation (lowest *p*-values) included tracts that pass through the temporal lobe, and posterior brain regions. The left hippocampal component of the cingulum showed consistently high effect sizes for distinguishing groups, across all diffusivity and anisotropy measures, and in correlations with cognitive scores.

1. Introduction

Alzheimer's disease (AD) is the most common type of dementia, affecting 1 in 8 people over age 65 in the U.S. alone (Alzheimer's Disease Association, 2012). Its prevalence is predicted to more than double in the next 40 years (Hebert et al., 2003). It is important to identify individuals most likely to develop AD, so that those at greater risk can be treated earlier. One high-risk group consists of people with mild cognitive impairment (MCI) — a transitional stage between normal aging and AD. People with MCI convert to AD at a rate of about 10–15% per year (Petersen et al., 2001; Bruscoli and Lovestone, 2004). In addition to the more widely-accepted measures from anatomical MRI, PET, and CSF measures of pathology, one major neuroimaging study of AD – the Alzheimer's Disease Neuroimaging Initiative (ADNI) – recently incorporated additional neuroimaging techniques including diffusion tensor imaging (DTI) (Jack et al., 2010; Jahanshad et al., 2010a; Zhan et al., in press). DTI is a variant of MRI that measures the diffusion of water molecules in brain tissue. Here we set out to assess which standard DTI measures may best identify neuroanatomical differences between AD, MCI, and normal aging. In the end, DTI offers a range of measures that might be sensitive to pathology, including measures of brain connectivity (Daianu et al., 2012, 2013a,b; Nir et al., 2012; Prasad et al., 2013; Toga and Thompson, 2013). For these initial analyses, however, we aimed to analyze more traditional measures and maps that are perhaps most likely to be used in standardized multi-site DTI analyses, at least in the near future (Jahanshad et al., 2013).

Abbreviations: NC, normal control; RD, radial diffusivity; AxD, axial diffusivity; ADNI, Alzheimer's Disease Neuroimaging Initiative.

* Corresponding author at: Imaging Genetics Center, Laboratory of Neuro Imaging, 225E Neuroscience Research Bldg, 635 Charles Young Drive, Los Angeles, CA 90095, USA. Tel.: +1 310 206 2101; fax: +1 310 206 5518.
E-mail address: thompson@loni.ucla.edu (P.M. Thompson).

[1] Many investigators within the ADNI contributed to the design and implementation of ADNI and/or provided data, but most of them did not participate in the analysis or writing of this report. A complete list of ADNI investigators may be found at: http://adni.loni.ucla.edu/wp-content/uploads/how_to_apply/ADNI_Acknowledgement_List.pdf.

2213-1582/$ – see front matter © 2013 The Authors. Published by Elsevier Inc. All rights reserved.
http://dx.doi.org/10.1016/j.nicl.2013.07.006

MRI-based image analysis methods have long been used to track structural atrophy of the aging brain. MRI studies of AD reveal widespread neuronal loss and atrophy in the brain's gray matter, especially in medial temporal and hippocampal regions (Atiya et al., 2003; Chetelat and Baron, 2003; Thompson et al., 2003; Anderson et al., 2005; Apostolova and Thompson, 2008; Bakkour et al., 2009; Risacher et al., 2009; Apostolova et al., 2010; Desikan et al., 2010a; Desikan et al., 2010b; Chiang et al., 2011; Weiner et al., 2012; Leung et al., 2013). Beta-amyloid and tau proteins accumulate in the brain, leading to inflammation, neuronal atrophy and cell death (Braak and Braak, 1991; Braak and Braak, 1995). As neurons are lost, white matter volume is also reduced, due to both myelin degeneration and axon loss in neural fiber tracts (Braak and Braak, 1996; Bartzokis, 2011; Braskie et al., 2011; Hua et al., 2013). Standard anatomical MRI is still the imaging technique most often used in AD studies and clinical trials, but DTI is sensitive to microscopic changes in white matter (WM) integrity not always detectable with standard anatomical MRI (Xie et al., 2006; Canu et al., 2010). Although this is debatable until more evidence is collected, some DTI changes may even precede and predict volume loss (Hugenschmidt et al., 2008; Nir et al., 2012), making it a potentially beneficial tool for capturing additional or complementary markers of early neurodegeneration. Carriers of some AD risk genes show differences on DTI as young adults, decades before the typical age of onset of AD (Braskie et al., 2011).

Fractional anisotropy (FA) is perhaps the most widely accepted DTI measure and reflects how directionally constrained the diffusion of water is along axons. While higher FA values may imply more coherent or intact axons, or a higher degree of myelination, lower FA may reflect loss of WM integrity and injury. These physiological correlates of the DTI signal are widely accepted, but the differences may have other interpretations, especially where fibers cross (Leow et al., 2009; Zhan et al., 2009). Mean diffusivity (MD) captures the average rate of diffusion in all directions, and generally increases with WM injury, especially if normal barriers to diffusion are damaged (such as myelin sheaths on axons). Axial diffusivity (AxD) captures diffusion parallel to axonal fibers, while radial diffusivity (RD) reflects perpendicular diffusion. These measures are linked to axonal injury and demyelination, respectively (Song et al., 2003; Song et al., 2005). To date, numerous DTI studies of AD and MCI find that greater cognitive impairment, or poorer diagnosis, is associated with lower FA in the corpus callosum, fornix, cingulum, superior longitudinal fasciculus, and inferior longitudinal fasciculus (Ukmar et al., 2008; Stricker et al., 2009; Mielke et al., 2009; Liu et al., 2011) and DTI measures correlate with widely used clinical or cognitive ratings including the mini-mental state exam (MMSE) (Bozzali et al., 2002).

Despite growing diffusion imaging evidence of AD-related WM changes, it is not clear which regions and DTI measures are the most sensitive for detecting diagnostic differences. In order to evaluate the power of drug trial treatment to counteract degeneration, optimizing statistical power for discerning differences and changes is crucial. We focused this current paper on cross-sectional differences in patients and controls, as there are a number of DTI measures, regions, and approaches that need to be compared and ranked in terms of their effect sizes for picking up group differences. We set out to rank the effect sizes for different DTI-based scalar measures in detecting differences in both white matter voxel-based analyses (VBA) and within regions of interest (ROIs). We first examined differences in DTI anisotropy and diffusivity measures between groups of cognitively healthy normal elderly controls (NC), MCI, and AD patients in both voxel-based and ROI analyses. We also examined the association of anisotropy and diffusivity maps with widely used clinical or cognitive ratings including the MMSE (Folstein et al., 1975), the "sum-of-boxes" clinical dementia rating (CDR-sob) (Berg, 1988), and the Alzheimer's Disease Assessment Scale-Cognitive (ADAS-cog) (Rosen et al., 1984). Finally, in a supplementary test, we compared our ROI results to ROIs extracted along the skeleton from the widely used tract-based spatial statistics (TBSS) method (Smith et al., 2006). Despite the popularity of FA, we hypothesized that we would find the highest effect size and discriminative power for MD measures, as recently suggested in a review of DTI studies of AD by Clerx et al. (Clerx et al., 2012). We also hypothesized that we would find the greatest differences in temporal lobe WM and the corpus callosum (CC), as the temporal lobe is usually the earliest region to be affected by amyloid and tau pathology in AD, and DTI studies are often better powered to find group differences in regions such as the CC where fiber coherence is highest.

2. Materials and methods

2.1. Clinical sample and demographics

Baseline MRI, DTI, clinical, and neuropsychological data were downloaded from the ADNI database (http://adni.loni.ucla.edu). When the analysis was performed (September 2012), data collection for the ADNI2 project was still in progress. Here we performed an initial analysis of 155 participants from 14 data acquisition sites, of whom 44 were normal controls (NC), 88 amnestic MCI subjects, and 23 AD patients (see Inline Supplementary Table S1 for distribution of subjects across sites). Unlike ADNI1, ADNI2 MCI participants include the enrollment of a new early MCI cohort (e-MCI; $n = 62$), with milder episodic memory impairment than the MCI group of ADNI1. The MCI group of ADNI1 is now referred to as late MCI (l-MCI; $n = 26$) in ADNI2. Levels of MCI (early or late) were determined using the Wechsler Memory Scale — Logical Memory II (Wechsler, 1987). We evaluated the l-MCI and e-MCI groups both separately and as one large MCI group. Detailed inclusion and exclusion criteria are found in the ADNI2 protocol (http://adni-info.org/Scientists/Pdfs/ADNI2_Protocol_FINAL_20100917.pdf).

Inline Supplementary Table S1 can be found online at http://dx.doi.org/10.1016/j.nicl.2013.07.006.

Each subject underwent cognitive evaluations. The Mini-Mental State Examination (MMSE) was used to provide a global measure of cognitive status, based on evaluating cognitive domains including orientation to place, orientation to time, registration, attention and concentration, recall, language, and visual construction (Folstein et al., 1975). The total score ranges from 1 to 30, with lower scores indicating impairment. The Clinical Dementia Rating (CDR) was also used as a global measure of dementia severity (Berg, 1988). The "sum-of-boxes" CDR (CDR-sob) score is the sum of 6 measures each assessing the degree of impairment in memory, orientation, judgment and problem solving, community affairs, home and hobbies, and personal care. The CDR-sob score ranges from 0 to 18 (no dementia to severe dementia, respectively). Finally, the Alzheimer's Disease Assessment Scale-Cognitive (ADAS-cog), a global measure encompassing memory, reasoning, language, orientation, ideational, praxis and constructional praxis (Rosen et al., 1984), was collected where scores range from 0 to 70 (no dementia to severe dementia respectively). In *post-hoc* analyses, we further homed in on specific cognitive domains using the available ADNI composite scores for executive function (ADNI-EF) (Gibbons et al., 2012) and memory (ADNI-MEM) (Crane et al., 2012) derived using data from the ADNI neuropsychological battery. Detailed psychometric calculation protocols are available for download at https://ida.loni.ucla.edu/. ADNI-EF was calculated using a combination of WAIS-R Digit Symbol Substitution, Digit Span Backwards, Trails A and B, Category Fluency, and Clock Drawing scores (Gibbons et al., 2012), and ADNI-MEM was calculated as a composite of the Rey Auditory Verbal Learning Test (RAVLT), ADAS-Cog, and Logical Memory data (Crane et al., 2012).

Demographics and diagnostic information for the participants are shown in Table 1. Diagnostic groups did not differ in age, however, education, an AD risk factor (Sattler et al., 2012), was marginally significant between controls and AD. As would be expected, clinical measures that index cognitive decline (MMSE, ADAS-cog, CDR-sob, ADNI-MEM, ADNI-EF) did show significant graded differences between groups.

We further assessed whether these measures revealed more fine-grained differences between the l-MCI and e-MCI subgroups. We found

Table 1
Demographics and clinical scores for the participants.

	NC	MCI	e-MCI	l-MCI	AD	*p*-value for group difference			
	(n = 44)	(n = 88)	(n = 62)	(n = 26)	(n = 23)	NC vs MCI	MCI vs AD	e-MCI vs l-MCI	NC vs AD
Age	72.7 ± 5.9	73.3 ± 7.3	74.0 ± 7.9	71.8 ± 5.3	75.8 ± 10.0	0.59	0.27	0.15	0.17
Sex	22 M/22 F	53 M/35 F	38 M/24 F	15 M/11 F	15 M/8 F	–	–	–	–
Education	16.6 ± 2.7	15.9 ± 2.7	15.8 ± 2.8	16.2 ± 2.5	15.0 ± 3.0	0.18	0.22	0.50	0.05
MMSE	28.9 ± 1.3	27.8 ± 1.6	28.0 ± 1.5	27.5 ± 1.8	23.0 ± 1.9	**1.01E−4**	**4.90E−12**	0.24	**1.57E−14**
ADAS-cog[a]	5.3 ± 2.9	9.6 ± 4.2	8.4 ± 3.7	12.7 ± 4.0	20.4 ± 7.3	**2.90E−9**	**2.04E−6**	**1.45E−4**	**1.04E−8**
CDR-sob	0.03 ± 0.1	1.3 ± 0.7	1.2 ± 0.6	1.4 ± 0.9	4.96 ± 1.4	**1.38E−27**	**2.69E−12**	0.27	**2.68E−14**
ADNI-MEM[b]	0.84 ± 0.52	0.22 ± 0.46	0.36 ± 0.42	−0.12 ± 0.38	−0.74 ± 0.68	**1.01E−8**	**4.14E−6**	**5.97E−6**	**3.64E−10**
ADNI-EF[b]	0.79 ± 0.74	0.16 ± 0.64	0.14 ± 0.61	0.19 ± 0.73	−0.86 ± 0.87	**1.65E−5**	**5.16E−5**	0.75	**2.51E−8**

Bold entries signify $p < 0.05$.
[a] ADAS-cog data were available only for a subset of the subjects, with the following numerical breakdown: NC n = 41, MCI n = 78 (e-MCI = 57, l-MCI = 21), AD n = 20.
[b] ADNI-MEM and ADNI-EF composite scores were available only for a subset of the subjects, with the following numerical breakdown: NC n = 41, MCI n = 82 (e-MCI = 58, l-MCI = 24), AD n = 20.

differences in ADAS-cog scores — a measure developed specifically for Alzheimer's disease, and the most widely used primary outcome measure in clinical trials that test AD drug treatment efficacy (Mohs et al., 1983). ADNI-MEM was also significantly different as it is calculated using both ADAS-cog and Logical Memory data, the measure used to initially classify the two MCI subgroups.

2.2. MRI and DTI scanning

All subjects underwent whole-brain MRI scanning on 3 Tesla GE Medical Systems scanners at 14 acquisition sites across North America. Anatomical T1-weighted SPGR (spoiled gradient echo) sequences (256 × 256 matrix; voxel size = 1.2 × 1.0 × 1.0 mm^3; TI = 400 ms; TR = 6.98 ms; TE = 2.85 ms; flip angle = 11°), and diffusion-weighted images (DWI; 256 × 256 matrix; voxel size: 2.7 × 2.7 × 2.7 mm^3; TR = 9000 ms; scan time = 9 min; more imaging details can be found at http://adni.loni.ucla.edu/wp-content/uploads/2010/05/ADNI2_GE_3T_22.0_T2.pdf) were collected. 46 separate images were acquired for each DTI scan: 5 T2-weighted images with no diffusion sensitization (b_0 images) and 41 diffusion-weighted images (b = 1000 s/mm^2). This protocol was chosen after conducting a detailed comparison of several different DTI protocols, to optimize the signal-to-noise ratio in a fixed scan time (Jahanshad et al., 2010a; Zhan et al., in press). All T1-weighted MR and DWI images were checked visually for quality assurance to exclude scans with excessive motion and/or artifacts; all scans were included.

2.3. Image analysis

2.3.1. Preprocessing steps

For each subject, all raw DWI volumes were aligned to the average b_0 image (DTI volume with no diffusion sensitization) using the FSL *eddy_correct* tool (www.fmrib.ox.ac.uk/fsl) to correct for head motion and eddy current distortions. All extra-cerebral tissue was roughly removed from the T1-weighted anatomical scans using a number of software packages, primarily ROBEX, a robust automated brain extraction program trained on manually "skull-stripped" MRI data (Iglesias et al., 2011) and FreeSurfer (Fischl et al., 2004). Skull-stripped volumes were visually inspected, and the best one selected and sometimes further manually edited. Anatomical scans subsequently underwent intensity inhomogeneity normalization using the MNI *nu_correct* tool (www.bic.mni.mcgill.ca/software/). Non-brain tissue was also removed from the diffusion-weighted images using the Brain Extraction Tool (BET) from FSL (Smith, 2002). To align data from different subjects into the same 3D coordinate space, each T1-weighted anatomical image was linearly aligned to a standard brain template (the downsampled Colin27 (Holmes et al., 1998): 110 × 110 × 110, with 2 mm isotropic voxels) using FSL *flirt* (Jenkinson et al., 2002) with 6 degrees of freedom (dof) to allow translations and rotations in 3D. To correct for echo-planar imaging (EPI) induced susceptibility artifacts, which can cause distortions at tissue–fluid interfaces, skull-stripped b_0 images were linearly aligned (FSL *flirt*, 9 dof) and then elastically registered to their respective T1-weighted structural scans using an inverse-consistent registration algorithm with a mutual information cost function (Leow et al., 2007) as described in (Jahanshad et al., 2010b). The resulting 3D deformation fields were then applied to the remaining 41 DWI volumes prior to estimating diffusion parameters. To account for the linear registration of the DWI images to the structural T1-weighted scan, a corrected gradient table was calculated.

2.3.2. DTI maps

A single diffusion tensor (Basser et al., 1994), or ellipsoid, was modeled at each voxel in the brain from the eddy- and EPI-corrected DWI scans using FSL *dtifit*, and scalar anisotropy and diffusivity maps were obtained from the resulting diffusion tensor eigenvalues (λ_1, λ_2, λ_3) which capture the length of the longest, middle, and shortest axes of the ellipsoid. The tensor model in DTI has limitations, especially in regions where fibers cross, but we do not investigate it further here; our other papers consider this in more detail (Zhan et al., 2008; Leow et al., 2009; Zhan et al., 2009; Zhan et al., 2010; Zhan et al., 2011; Zhan et al., 2012b; Zhan et al., in press). Fractional anisotropy (FA), a measure of the degree of diffusion anisotropy, was calculated from the standard formula:

$$FA = \sqrt{\frac{3}{2}}\frac{\sqrt{(\lambda_1 - <\lambda>)^2 + (\lambda_2 - <\lambda>)^2 + (\lambda_3 - <\lambda>)^2}}{\sqrt{\lambda_1^2 + \lambda_2^2 + \lambda_3^2}} \in [0, 1]$$

$$<\lambda> = \frac{\lambda_1 + \lambda_2 + \lambda_3}{3}$$

Table 2
Index of 43 ROIs from the WM tract atlas (Mori et al., 2008) followed by their abbreviations.

Genu of corpus callosum	GCC	Posterior thalamic radiation	PTR L,R
Body of corpus callosum	BCC	Sagittal stratum	SS L,R
Splenium of corpus callosum	SCC	External capsule	EC L,R
Full corpus callosum	CC	Cingulum (cingulate gyrus)	CGC L,R
Corticospinal tract	CST L,R	Cingulum (hippocampus)	CGH L,R
Cerebral peduncle	CP L,R	Fornix (*crus*)/*Stria terminalis*	FX/ST L,R
Anterior limb of internal capsule	ALIC L,R	Superior longitudinal fasciculus	SLF L,R
Posterior limb of internal capsule	PLIC L,R	Superior fronto-occipital fasciculus	SFO L,R
Retrolenticular part of internal capsule	RLIC L,R	Inferior fronto-occipital fasciculus	IFO L,R
Anterior *corona radiata*	ACR L,R	Uncinate fasciculus	UNC L,R
Superior *corona radiata*	SCR L,R	*Tapetum*	TAP L,R
Posterior *corona radiata*	PCR L,R	All ROIs	TOTAL

- where <λ> is the mean diffusivity (MD), or average rate of diffusion in all directions. Axial diffusivity was defined as the primary (largest) eigenvalue (AxD = λ_1), and captures the longitudinal diffusivity, or the diffusivity parallel to axonal fibers (assuming of course that the principal eigenvector is indeed following the dominant fiber direction, which may be unclear in regions with extensive fiber crossing). Radial diffusivity (RD), which captures the average diffusivity perpendicular to axonal fibers, was calculated as the average of the two smaller eigenvalues:

$$RD = \frac{\lambda_2 + \lambda_3}{2}.$$

2.3.3. White matter tract atlas ROI summary measures

We linearly, then elastically registered (Leow et al., 2007) the FA image from the Johns Hopkins University (JHU) DTI atlas (Mori et al., 2008) to each subject's distortion corrected FA image. We then applied that deformation to the stereotaxic JHU "Eve" atlas WM labels (http://cmrm.med.jhmi.edu/cmrm/atlas/human_data/file/AtlasExplanation2.htm), using nearest neighbor interpolation to avoid intermixing of labels. This is not the atlas that had the problem pointed out by Rohlfing (2013). We then superimposed the atlas ROIs into the same coordinate space as our results. We removed 10 ROIs from the analyses (including the left and right middle cerebellar peduncle, pontine crossing tract, medial lemniscus, inferior and superior peduncles) as they often fell partially or completely out of the field-of-view (FOV) of the images. We also excluded the body of the fornix as it is small and prone to misregistration and partial voluming. AD researchers are specifically interested in the fornix as it is the primary posterior pathway coming out of the back of the hippocampus, a key target of pathology. While we included the crus of the fornix/*stria terminalis*, the body is just too small to be resolved well on DTI at this resolution. In addition to the JHU labels, 4 more ROIs were evaluated: bilateral genu, body, and splenium of the corpus callosum (as opposed to just the lateralized measures), as well as the entire corpus callosum, and a large "TOTAL" WM ROI made up of all the other ROIs, to obtain total summary measures of these regions. We were then able to calculate the average FA, MD, RD and AxD, within the boundaries of each of the 43 ROIs for each subject (Table 2).[2]

2.3.4. TBSS tract atlas ROI summary measures

Tract-based spatial statistics (TBSS) (Smith et al., 2006), provided in the FSL software package (http://www.fmrib.ox.ac.uk/fsl/), was also performed according to protocols outlined by the ENIGMA-DTI group: http://enigma.loni.ucla.edu/ongoing/dti-working-group/. All subjects' corrected FA maps were linearly, then elastically registered (Leow et al., 2007) to the ENIGMA-DTI template in ICBM space. The resulting 3D deformation fields were then applied to the three diffusivity maps. All subjects' spatially normalized FA, MD, RD and AxD data were projected onto the skeletonized ENIGMA-DTI template. Mean anisotropy and diffusivity measures were calculated along the skeleton in the same 43 ROIs (Table 2). This type of analysis has been used previously in both genetic studies and studies of disease to home in on associated WM tracts (Kochunov et al., 2011; Jahanshad et al., 2013).

2.3.5. Template creation and spatial normalization

A study-specific minimal deformation template (MDT) (Gutman et al., 2012) was created using 29 cognitively healthy elderly control (NC) spatially aligned FA maps. An MDT deviates, on average, the least (in some metric) from the anatomy of the subjects, and can often improve registration accuracy and statistical power (Gutman et al., 2012; Lepore et al., 2007). The MDT was generated by creating an initial affine mean template from all 29 subjects, then registering all the aligned individual scans to that mean using a fluid registration (Leow et al., 2007) while regularizing the Jacobians (Yanovsky et al., 2007). A new mean was created from the registered scans; this process was iterated several times. Each subject's initial FA map was elastically registered to the final MDT and the resulting deformation fields were applied to the 3 diffusivity maps to align them to the same coordinate space. To ensure white matter alignment across subjects, registered FA maps were thresholded at FA > 0.2 to include only highly anisotropic anatomy and the thresholded maps were elastically registered to the thresholded MDT (FA > 0.2). Again, the resulting deformation fields were applied to all previously registered DTI maps. We also used the tissue-specific, smoothing-compensated method (*T-SPOON*) proposed by Lee et al. (2009) to improve tissue specificity and reduce confounds caused by morphometric differences that are not fully corrected by the elastic registration.

2.4. Statistical analysis

We ran voxel-wise multiple linear regressions, covarying for age and sex, to test for statistical effects of AD and MCI diagnosis relative to the NC group, on measures of white matter integrity in FA, MD, RD, and AxD maps. We also tested for associations between these DTI measures and MMSE, CDR-sob, and ADAS-cog scores, controlling for age and sex, across the entire study sample (i.e., including all AD, MCI and NC subjects), and also within each subgroup. We also ran all of the regressions using a random-effects regression model, grouping the data by acquisition site. To limit statistical testing to white matter, where the power is greater to detect differences, statistics were run only on voxels within the boundaries of the MDT thesholded at FA > 0.2. Prior studies have thresholded FA values between 0.2 and 0.3 to successfully exclude gray matter or CSF (Wakana et al., 2005; Smith et al., 2006). As we were studying a clinical population, we chose the more conservative (lower) limit of the recommended FA threshold. We also only ran statistics on voxels of the thresholded MDT present in all subject scans, as some scans had a slightly cropped FOV. As such, we did not consider the inferior parts of the cerebellum and brain stem.

We ran random-effects regressions on the average anisotropy and diffusivity measures within the 43 full ROIs, again covarying for age and sex, testing for statistical effects of diagnosis (NC vs. MCI, or AD), 3 global clinical test scores, and *post-hoc* tests on ADNI-MEM and ADNI-EF. We further tested and compared TBSS ROI measures.

Computing multiple association tests for each ROI, or thousands of tests on a voxel-wise level can introduce a high false positive error rate. To account for these errors, we used the standard false discovery rate (FDR) method to control the false positive rate of each map at $q = 0.05$ (Benjamini and Hochberg, 1995). All statistical maps shown in this paper (Figs. 1–5) were thresholded at the FDR critical *p*-value.

To visualize and compare effect sizes in the anisotropy and diffusivity maps, we computed and graphed the cumulative distribution functions (CDF) of the *p*-values obtained from the voxel-wise and ROI random-effects regressions. The ordered set of observed *p*-values was plotted against the expected null distribution. If there are no group differences (a null distribution), then the plot would fall approximately along the $y = x$ diagonal line. However, if the CDF initially rises at a rate steeper than 20 times the null CDF ($y = 20x$), then the corresponding maps are FDR significant at $q = 0.05$. A greater slope reflects a larger effect size; the FDR critical *p*-value (at $q = 0.05$) is the point at which the curve intersects the $y = 20x$ line.

DTI measures calculated from a single-tensor diffusion model have limitations in regions with extensive fiber crossing. For example, in AD we might expect FA deficits throughout the brain, but FA may appear to be artificially *increased* where crossing fibers deteriorate (Douaud et al., 2011). To make sure that these results were not false positives we separated the full *p*-value map (irrespective of the significance level of the voxels) into two maps: (1) voxels that showed a negative association, and (2) positively associated voxels. We then independently

[2] Except for the total WM ROI, all these ROI measures for all subjects are available for download at https://ida.loni.ucla.edu/.

corrected each *p*-map for multiple statistical comparisons using FDR (Benjamini and Hochberg, 1995).

As an alternative way to visualize white matter integrity differences between patients and controls, we also created maps showing the "percent difference" in mean DTI measures between AD patients and NC, within the FDR significant regions.

$$\%Diff = \frac{\overline{AD} - \overline{NC}}{\overline{NC}}.$$

There is a mild bias in doing this, in that it selects voxels that show effects, and then computes the magnitude of the effects. Even so, it was used to simply describe how much difference was seen in the regions shown, bearing in mind that the same difference would not be found in the rest of the brain.

3. Results

3.1. Voxel-based analyses

3.1.1. White matter integrity differences between diagnostic groups

3.1.1.1. AD vs controls. As measured by FA, AD patients showed pervasive deficits in fiber integrity (lower FA) compared to healthy controls, throughout the WM across the entire brain, when using a general linear regression model to adjust for age and sex (critical $p < 0.016$; 31.9% of voxels survived the FDR threshold (Benjamini and Hochberg, 1995); minimum *p*-value, 1.65×10^{-8}). However, when we used a random-effects regression model at every voxel to take into account acquisition site differences, we found more significant and even more widespread results (critical $p < 0.020$; 40.1% of voxels survived the FDR threshold (Benjamini and Hochberg, 1995); minimum *p*-value, 6.66×10^{-9}; Fig. 1a). We therefore proceeded with this model – fitting a site effect – for the remainder of the analyses. A few significant voxels exhibited associations in a direction opposite to the great majority of the brain map, and contrary to what would traditionally be accepted as showing impairment. For example, we found regions where the AD group had a higher mean FA (Fig. 1e; *blue regions*). These regions were largely found at the junction of the corpus callosum commissural fibers and the *corona radiata*. Such regions are notorious for fiber crossings, which may artificially reduce FA, if FA is estimated using the single-tensor diffusion model (Oishi et al., 2011). This pattern has been reported in other AD studies, and may reflect a selective sparing or selective degeneration of one of the pathways in a region with crossing fibers (Douaud et al., 2011). When we separated (and independently FDR-corrected) the map of voxels that showed a negative association with AD and the map of the positively associated voxels, the diffuse negative associations were still significant, but the previously significant positive associations were not.

This pervasive pattern of significance was largely replicated for the three other diffusivity measures. As predicted, we found higher mean RD, AxD and MD values in AD patients relative to controls (Fig. 1 b–d) and the effects were larger and even more diffuse than for FA. CDF plots confirm that FA was not the most sensitive measure for differentiating groups. Comparisons of NC to AD patients (Fig. 2a) revealed that RD was the most sensitive measure followed closely by MD.

3.1.1.2. Early, late and all MCI vs controls. No significant difference was detected between e-MCI and l-MCI groups for any of the DTI measures, so we first assessed the MCI group as a whole, followed by these subgroups. We found no significant differences between NC and MCI as a whole ($n = 88$), or NC and the e-MCI ($n = 62$) subgroup, for any of the anisotropy or diffusivity measures. However, for NC compared to l-MCI subjects ($n = 26$), we did find significantly higher diffusivity measures in the left hippocampal part of the cingulum (MD: FDR critical $p < 3.05 \times 10^{-5}$; RD: FDR critical $p < 2.72 \times 10^{-5}$; AxD: FDR critical $p < 2.46 \times 10^{-5}$; Fig. 3). While these measures are significant on their own, the N was small. These contrasts will benefit from further analysis, as the ADNI dataset grows.

3.1.2. Correlation with MMSE, CDR-sob, and ADAS-cog neuropsychological scores

3.1.2.1. Full cohort. We first assessed anisotropy and diffusivity map associations with widely used clinical cognitive ratings in the entire study population, including AD patients, MCI, and NC subjects (Fig. 4). Fig. 4a shows WM regions where anisotropy and diffusivity differences correlated with the MMSE scores in the entire study population ($n = 155$). MMSE was significantly positively associated with FA (FDR critical $p < 0.018$), and negatively associated with diffusivity (MD: FDR critical $p < 0.037$; RD: FDR critical $p < 0.040$; AxD: FDR critical $p < 0.028$). That is, lower FA and higher diffusivity, which typically indicate greater WM deficits, were associated with lower MMSE scores, indicative of greater impairment. Fig. 4b shows WM regions where FA and diffusivity differences correlated with the CDR-sob scores ($n = 155$). As expected, FA was negatively associated with CDR-sob (FDR critical $p < 0.027$), and diffusivity was positively associated (MD: FDR critical $p < 0.039$; RD: FDR critical $p < 0.042$; AxD: FDR critical $p < 0.029$). Fig. 4c shows WM regions where FA was negatively associated with ADAS-cog ($n = 139$; FDR critical $p < 0.016$), and diffusivity positively associated (MD: FDR critical $p < 0.040$; RD: FDR critical $p < 0.041$; AxD: FDR critical $p < 0.029$). Lower FA and higher diffusivity were associated with higher (*worse*) ADAS-cog and CDR-sob scores. CDF plots of MMSE, ADAS-cog, and CDR-sob voxel-wise associations again reveal that FA associations, while FDR significant, show the smallest effect size, while MD and RD have the largest effect sizes (Fig. 2d).

As with diagnostic group differences, in all clinical score analyses we found small significant regions with associations in a direction opposite to what would traditionally be accepted as showing impairment. Again, when we corrected for multiple comparisons on voxel-wise *p*-maps of each association direction separately, the associations in the unexpected direction were no longer significant and only the intuitive direction remained.

3.1.2.2. Early, late and all MCI. We further assessed associations between cognitive scores and DTI measures in just the MCI group, as well as e-MCI and l-MCI subgroups. We found a significant positive association between all three diffusivity measures and CDR-sob within the MCI group (MD: FDR critical $p < 0.006$; RD: FDR critical $p < 0.006$; AxD: FDR critical $p < 0.002$; Fig. 5) and a small positive association between ADAS-cog and MD in the middle or lateral occipital WM in l-MCI (FDR critical $p < 5.35 \times 10^{-6}$). However, there was no detectable association with anisotropy or diffusivity measures and MMSE scores.

3.2. ROI analyses

3.2.1. ROI differences between diagnostic groups

3.2.1.1. AD vs controls. We sorted the JHU atlas ROI results by *p*-value to assess which ROIs showed the greatest differences between groups. In doing so, we have to bear in mind that this is not a ranking of the disease effects on the brain by severity; results may also be affected by how accurately each region can be measured, which in turn depends on the size and the homogeneity of the region. With these caveats in mind, Tables 3–4 list the 'top 10' most significant ROIs for each regression analysis (here and in what follows, we use the term 'most significant' to mean lowest *p*-values in the tests of group differences in mean values; we acknowledge that this term is not always preferred by statisticians as the *p*-values from different tests cannot necessarily be compared). When comparing NC to AD patients (Table 3a), the splenium of the corpus callosum, left fornix (*crus*)/*stria terminalis*, left hippocampal part of the cingulum, and total ROI map, were in the top 10 most

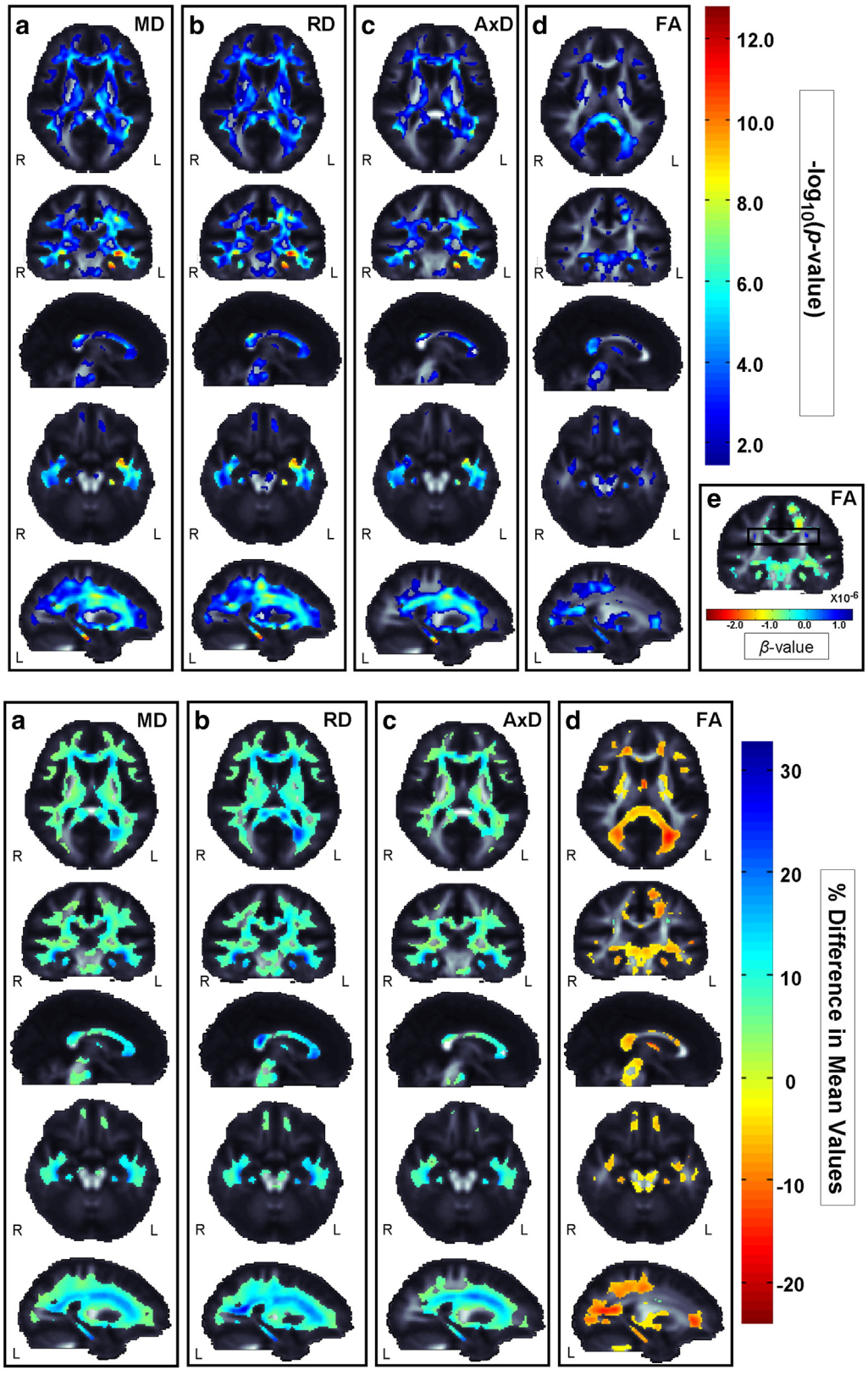

Fig. 1. (Top panels) Statistical maps show $-\log_{10} p$-values within regions where AD patients exhibit significantly *higher* (a) MD (FDR critical $p < 0.038$), (b) RD (FDR critical $p < 0.041$), and (c) AxD (FDR critical $p < 0.027$) than healthy controls (NC). The cingulum, temporal lobe (including the hippocampal part of the cingulum) and splenium of the corpus callosum show the "most significant" differences, i.e. greatest effect sizes in the maps. (d) Significant but slightly less profuse FA differences between groups were also found (FDR critical $p < 0.020$). (e) *Beta*-values (non-normalized slope of the regression) within FDR significant regions largely revealed regions with *lower* FA in AD, but there are small regions, notorious for crossing fibers, where AD patients have higher mean FA than controls (*dark blue*), contrary to what would traditionally be accepted as showing impairment. (Bottom panel) Maps show the *percent difference* in FA and diffusivity measures between AD patients and NC within FDR significant regions. Again, the corpus callosum, temporal lobe, cingulum (including the hippocampal part of the cingulum), and the posterior thalamic radiations show the greatest degree of difference (up to ~33%); we note that the significance values and effect sizes in these regions depend on the mean group differences and its standard error, which is more completely reflected in top panels. In both figures, MD and RD differences are greater and more widespread. (For interpretation of the references to color in this figure legend, the reader is referred to the web version of this article.)

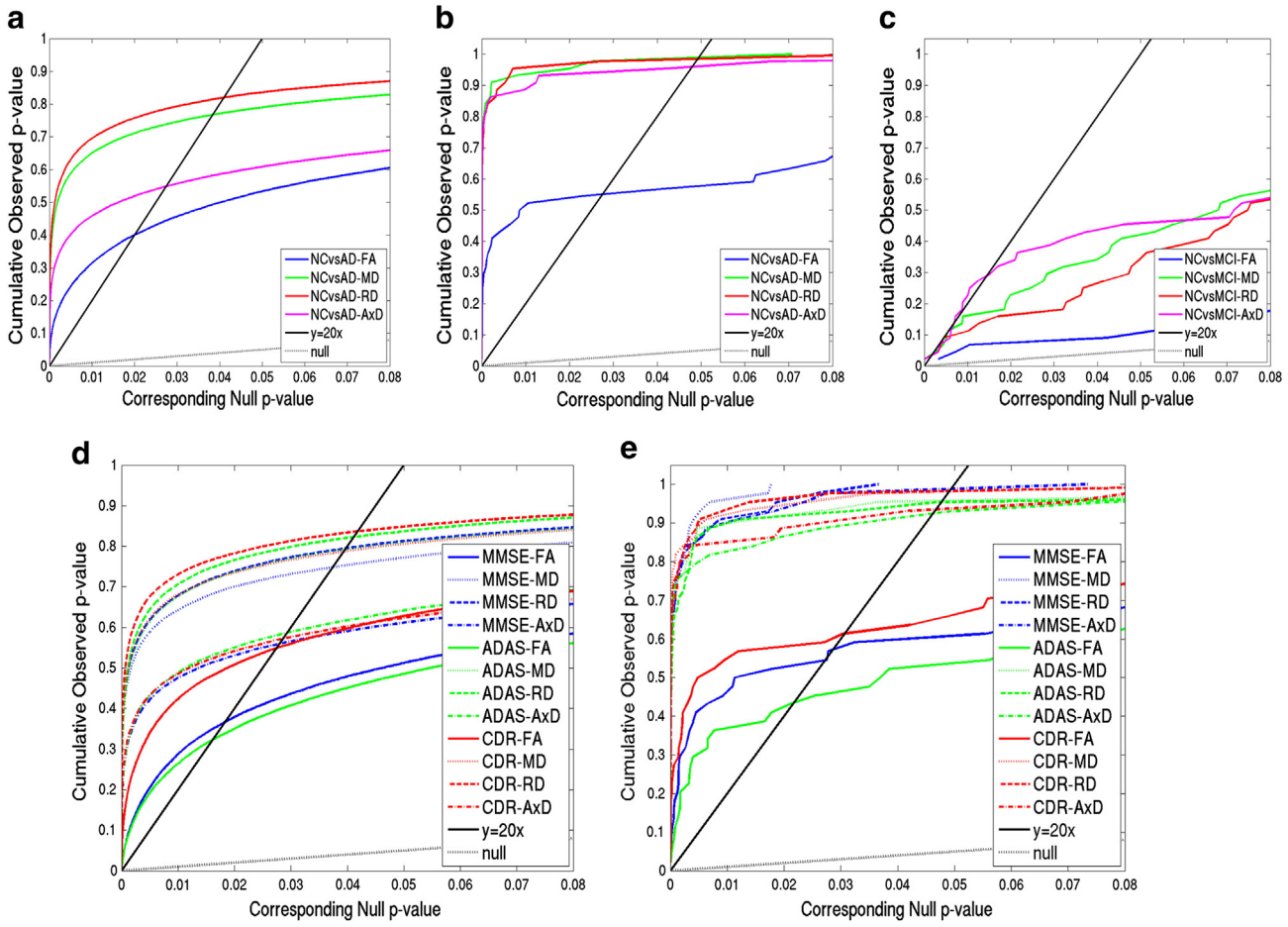

Fig. 2. Effect sizes for FA, MD, RD and AxD measures in AD, MCI and NC group comparisons and clinical cognitive test score associations reveal that FA is consistently the least sensitive measure. This type of plot is used to compare effect sizes in statistical maps based on different diffusivity measures. We used it to help decide which DTI measures best distinguish the diagnostic groups. Here we show cumulative distribution function (CDF) plots of the distribution of the *p*-values obtained from (a,d) voxel-wise and (b–c, e) ROI linear regressions, which are subjected to multiple comparisons correction using standard FDR (Benjamini and Hochberg, 1995). (a) VBA comparisons of NC to AD patients revealed that RD was the most sensitive measure (denoted by the higher critical *p*-values controlling the FDR, i.e., the highest non-zero *x*-coordinate where the CDF crosses the $y = 20x$ line) followed closely by MD. (b) ROI comparisons of NC vs AD confirm that FA was the *least sensitive* measure. (c) ROI comparisons of NC vs MCI reveal that AxD measures had the largest effect size, followed by MD (VBA comparisons were not significant). (d) Voxel-wise and (e) ROI linear regressions on associations between cognitive scores (MMSE, CDR-sob, and ADAS-cog) in the entire cohort and anisotropy and diffusivity measures confirm that FA associations, while FDR significant, show the smallest effect size, while MD and RD have the largest effect sizes.

significant ROIs, across all anisotropy and diffusivity measures. While the superior *corona radiata* and left sagittal stratum (which includes inferior longitudinal fasciculus and inferior fronto-occipital fasciculus) were in the top 10, across all diffusivity measures.

3.2.1.2. Early, late and all MCI. As there were no significant differences between l-MCI and e-MCI subjects across any of the measures, we compared the entire MCI group to NC subjects (Table 3b). While no ROI showed significant FA differences, the splenium of the corpus callosum, left *tapetum*, left hippocampal part of the cingulum, and left fornix (*crus*)/*stria terminalis* were in the top 10, among all diffusivity measures. We further assessed differences between e-MCI and NC and l-MCI and NC. The left hippocampal part of the cingulum was significant across all three diffusivity measures in both comparisons (Table 3c–d). FA showed no statistically significant differences.

CDF plots of the ROI *p*-values for NC vs AD (Fig. 2b) confirm VBA findings that FA was the least sensitive measure, and that RD has a slightly higher effect size than other measures. However, CDF plots of the ROI *p*-values, for NC vs MCI, reveal that AxD measures had the largest effect size, followed by MD (Fig. 2c). Table 3d also reveals that AxD has a larger effect size when comparing l-MCI and NC.

3.2.2. ROI correlations with clinical global neuropsychological scores

The strongest associations with MMSE score (Table 4a) across all four measures were found in the left hippocampal part of the cingulum, the left fornix (*crus*)/*stria terminalis*, and the total ROI map. All three diffusivity measures were additionally associated with MMSE in the left cingulum, and the bilateral sagittal stratum (this includes the inferior longitudinal fasciculus and inferior fronto-occipital fasciculus).

The strongest associations with CDR-sob score (Table 4b) across all four measures were found in the entire corpus callosum, the left hippocampal part of the cingulum, and the total ROI map. All three diffusivity measures additionally associated with CDR-sob in the left cingulum, and bilaterally in the sagittal stratum and inferior fronto-occipital fasciculus.

The strongest associations with the ADAS score (Table 4c) across all four measures were found in the left hippocampal part of the cingulum, and in all three diffusivity measures in the left cingulum, bilaterally in the sagittal stratum and inferior fronto-occipital fasciculus, and in the total ROI map.

As with voxel-wise measures, we further assessed the association between cognitive scores and ROI DTI measures in just the MCI group as a whole and also in the e-MCI and l-MCI groups separately (Table 5). As would be predicted, we found significant negative MMSE associations with diffusivity in both the MCI group and e-MCI subgroup

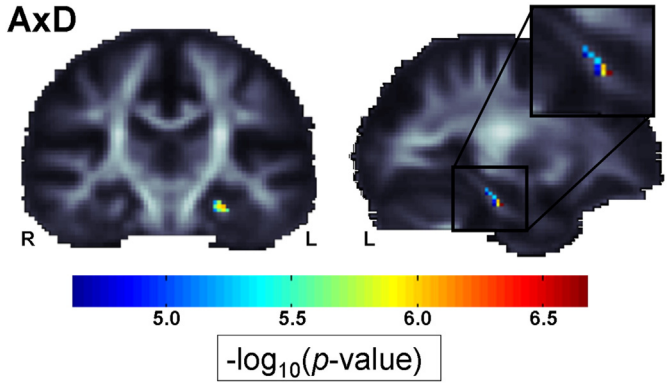

Fig. 3. Statistical maps show the $-\log_{10} p$-values within regions where l-MCI subjects exhibit significantly *higher* AxD (FDR critical $p < 2.46 \times 10^{-5}$) than healthy controls (NC). The left hippocampal part of the cingulum was also significant in MD and RD maps. This region is small, but it passes the conventional FDR correction for multiple comparisons, and is in a region implicated in early changes in AD (medial temporal regions). With a greater sample size, this effect may be detectable in the other hemisphere as well.

in the left hippocampal part of the cingulum. We found significant positive associations between MD and AxD and CDR-sob scores in the MCI group and no associations with ADAS-cog.

Again, CDF plots of the ROI *p*-values for cognitive score associations (Fig. 2b) confirm that FA was the least sensitive measure.

3.2.3. ROI analyses summary

ROIs that were consistently most significant across all three diffusivity measures in more than one analysis (Fig. 6) included the splenium of the CC, the left cingulum, particularly the hippocampal part, the left fornix (*crus*)/*stria terminalis* which projects to the dorsal region of the hippocampus, bilateral temporal lobe sagittal stratum, and the average measure across all ROIs. They also included the bilateral inferior fronto-occipital fasciculus in clinical score analyses. Of these ROIs, the left fornix (*crus*)/*stria terminalis* and hippocampal cingulum, and total ROI map were most significant across all anisotropy and diffusivity measures in at least two analyses. However, the left hippocampal part of the cingulum was in the top 10 ROIs in by far the most analyses.

For complete tables of TBSS ROI diagnostic group and cognitive score analyses results, please see Inline Supplementary Tables S2–S4. To summarize, TBSS ROIs that were consistently most significant (i.e., giving greatest effect sizes) across all four anisotropy and diffusivity measures in more than one analysis included the splenium of the CC, bilateral hippocampal part of the cingulum, the left sagittal stratum and uncinate, and the average measure across all ROIs (Inline Supplementary Fig. S1). While full ROI analyses additionally revealed bilateral inferior fronto-occipital fasciculus, left fornix (*crus*)/*stria terminalis*, left cingulum, and right sagittal stratum, as top ROIs and TBSS did not, TBSS ROIs additionally revealed the left uncinate and right hippocampal part of the cingulum. For a comparison of TBSS and full ROI analyses *p*-value CDF plots see Inline Supplementary Fig. S2.

Inline Supplementary Tables S2–S4, Figs. S1 and S2 can be found online at http://dx.doi.org/10.1016/j.nicl.2013.07.006.

3.2.4. Post-hoc ROI correlations with memory and executive function scores

The strongest associations between full ROI measures and ADNI-EF (Table 6a) in the entire study cohort (n = 143) across all four DTI measures were found in the bilateral sagittal stratum and the total ROI map. All three diffusivity measures were additionally associated with ADNI-EF in the bilateral cingulum, left hippocampal cingulum, and left superior longitudinal fasciculus.

There were no associations between FA and ADNI-MEM (Table 6b) in the entire cohort, but all three diffusivity measures were associated with ADNI-MEM bilaterally in the cingulum and hippocampal cingulum, bilateral inferior fronto-occipital fasciculus and sagittal stratum, and left uncinate and external capsule.

These measures were not linked to DTI measures in the MCI group as a whole, nor the e-MCI and l-MCI groups separately.

4. Discussion

In this ADNI study, we found that DTI indicators of white matter impairment have the potential to emerge as useful clinical tools for differentiating diagnostic groups in studies of AD. We had three main findings: (1) in ROI and VBA analyses, we found widespread anisotropy and diffusivity disruptions, often in tracts that pass through the temporal lobe and posterior brain regions (especially the left hippocampal cingulum), in elderly AD and MCI patients; (2) these disruptions were also associated with neuropsychological and cognitive deficits; and (3) diffusivity (MD, RD, AxD) measures were more sensitive for detecting differences than FA measures, and could detect more subtle MCI differences, where FA could not.

Alzheimer's disease (AD) is characterized by neuronal loss and widespread gray matter atrophy, but it is also marked by a disturbance in the brain's WM pathways, perhaps secondary to the effect of cortical neuronal loss. Changes in white matter neuropathology include partial loss of axons, myelin sheaths, and oligodendroglial cells (Brun and Englund, 1986; Sjobeck et al., 2005). AD patients have been shown to have significantly more WM hyperintensities (WMH) than controls. WMH are significantly related to cortical atrophy (Capizzano et al., 2004), entorhinal cortex (Guzman et al., in press) and hippocampal atrophy (de Leeuw et al., 2004) in AD patients. Significant WM atrophy has also been reported (Hua et al., 2008; Hua et al., 2010; Migliaccio et al., 2012).

There is growing diffusion imaging evidence of AD related WM changes as well. Most studies report lower FA and higher MD in all lobes of the brain in both MCI and AD when compared to cognitively healthy controls, with emphasis on medial temporal lobe structures (Kantarci et al., 2001; Bozzali et al., 2002; Takahashi et al., 2002; Fellgiebel et al., 2004; Medina et al., 2006; Rose et al., 2006; Xie et al., 2006; Zhang et al., 2007; Kavcic et al., 2008; Stebbins and Murphy, 2009), consistent with regions showing earliest pathological changes (Braak and Braak, 1991; Braak and Braak, 1995; Thompson et al., 2007) and our results. Many DTI methods have been used to assess WM differences in AD including TBSS (Smith et al., 2006) and tract or connectivity analyses (Daianu et al., 2012, 2013a,b). Here we use the most common methods, VBA and ROI analyses, with ROIs based on a stereotaxic WM ROI atlas (Mori et al., 2008), which has been shown to accurately parcellate anatomical regions in AD patients with severe atrophy (Oishi et al., 2009). Using predetermined, template-based ROIs can limit findings, and registration across subjects may vary due to morphological differences. However, using a common atlas helps to make quantification efficient and easier to standardize across sites (Jahanshad et al., 2013). Given that VBA findings are diffuse, ROIs are arguably helpful to begin to rank the most sensitive regions for detecting group differences.

When comparing AD patients to NC, the largest VBA differences were found in the corpus callosum (CC), temporal lobe, cingulum and hippocampal cingulum, and regions near the posterior thalamic radiations. ROI analyses revealed similar diffuse patterns with the CC splenium, the left fornix (*crus*)/*stria terminalis*, and average measure across all ROIs in the top 10 most significant (lowest p-values) ROIs across all anisotropy and diffusivity measures. However, we found that the most significant ROIs were not necessarily the most coherent tracts. Large clinical DTI studies with limited spatial and directional resolution are often better powered to find deficits in regions where the FA and fiber coherence is highest, such as the splenium of the CC. In a supplementary test, we assessed whether the ROI average FA values in the NC group was correlated with the effect size of each ROI (which is related to the *p*-values obtained) in the NC vs AD comparison (see supplementary text). Inline Supplementary Fig. S3 shows that the ROI

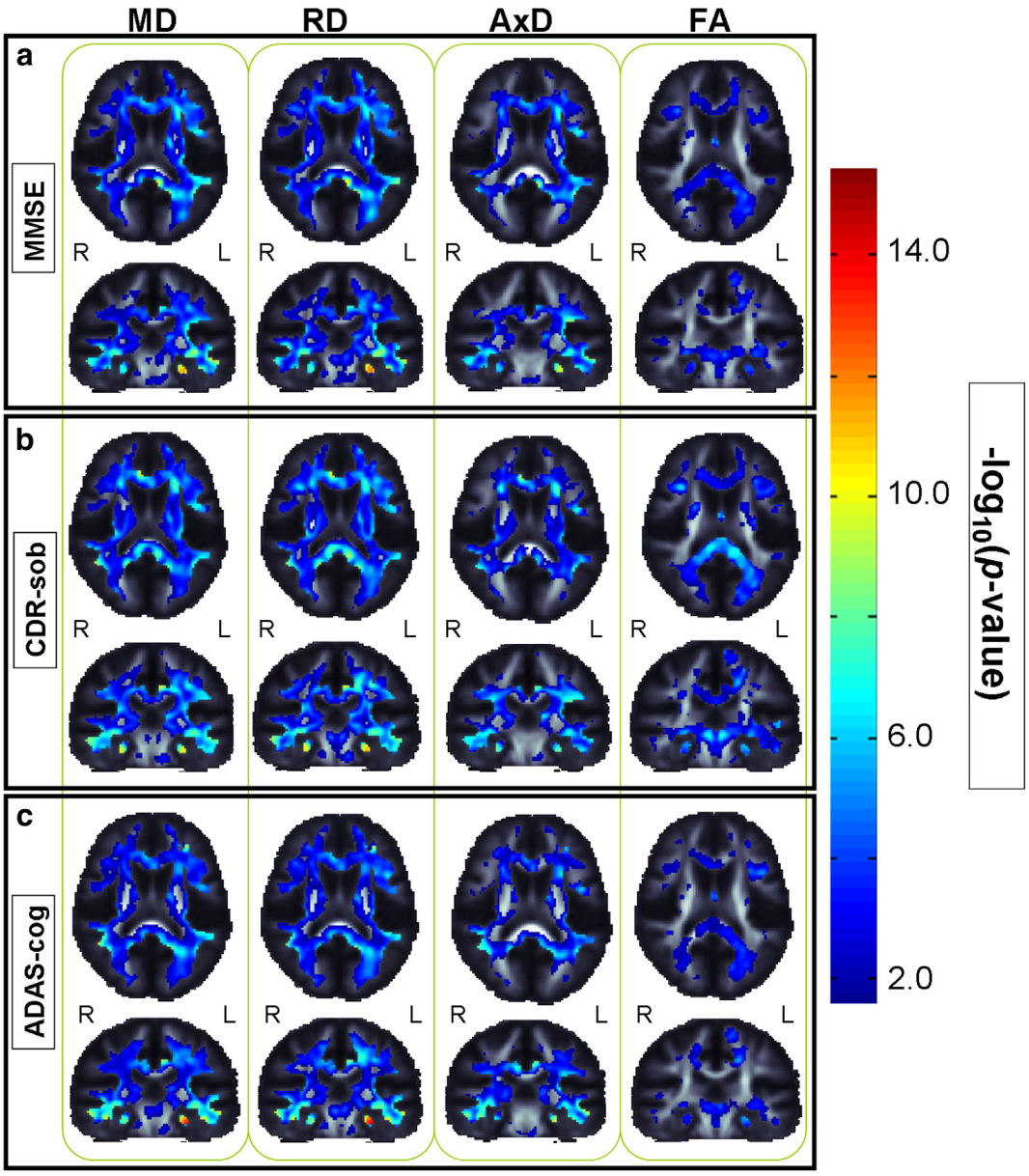

Fig. 4. Statistical maps show that clinical scores on the (a) MMSE, (b) CDR-sob, and (c) ADAS-cog are related to detectable differences in fractional anisotropy, and mean, radial and axial diffusivity in the entire cohort. These maps show the $-\log_{10}$ *p*-values within regions that significantly correlate with cognitive scores. RD and MD show the most widespread and robust associations. The hippocampal part of the cingulum and surrounding temporal lobes show the "most significant" associations (i.e., lowest *p*-values and highest voxel-wise effect sizes) between cognitive performance and white matter integrity.

average FA values in the NC group were not correlated with the effect size (defined by the Z-score corresponding to the *p*-values) of each ROI.

Only diffusivity measures were sensitive enough to detect more subtle differences between NC and MCI groups. ROIs including the splenium of the CC, left *tapetum*, left hippocampal part of the cingulum and left fornix (*crus*)/*stria terminalis* consistently differed in all diffusivity measures but not FA. Only the left hippocampal part of the cingulum was significant across all three diffusivity measures in both comparisons of e-MCI and l-MCI to controls. Similarly, only the left hippocampal part of the cingulum displayed significant increased diffusivity in l-MCI in the VBA analyses.

Inline Supplementary Fig. S3 can be found online at http://dx.doi.org/10.1016/j.nicl.2013.07.006.

The lack of larger differences between the MCI and normal control groups is surprising in light of other studies showing that these groups often differ on other neuroimaging measures. This may be due the small sample size and also heterogeneity in the MCI cohort. The MCI group referred to in papers using ADNI1 data is now called late MCI (l-MCI) in ADNI2. In ADNI2, the majority of the MCI group includes the enrollment of a new cohort called early MCI (e-MCI), with milder episodic memory impairment than the l-MCI group. Among the MCI subjects with DTI data available, a smaller percent will be l-MCI than in phase one of ADNI, perhaps contributing to the apparent discrepancy with other ADNI studies/results. This difference in the ADNI2 versus ADNI1 and other MCI cohorts should be considered in expectations of what the effect sizes should be.

Strongest ROI associations with cognitive scores in the full cohort were consistently found in the left hippocampal part of the cingulum across all anisotropy and diffusivity measures. The total ROI map was also one of the top 10 lowest *p*-values in almost all FA and diffusivity analyses, while left cingulum and bilateral sagittal stratum were in the top 10 in all diffusivity analyses. The bilateral inferior fronto-occipital

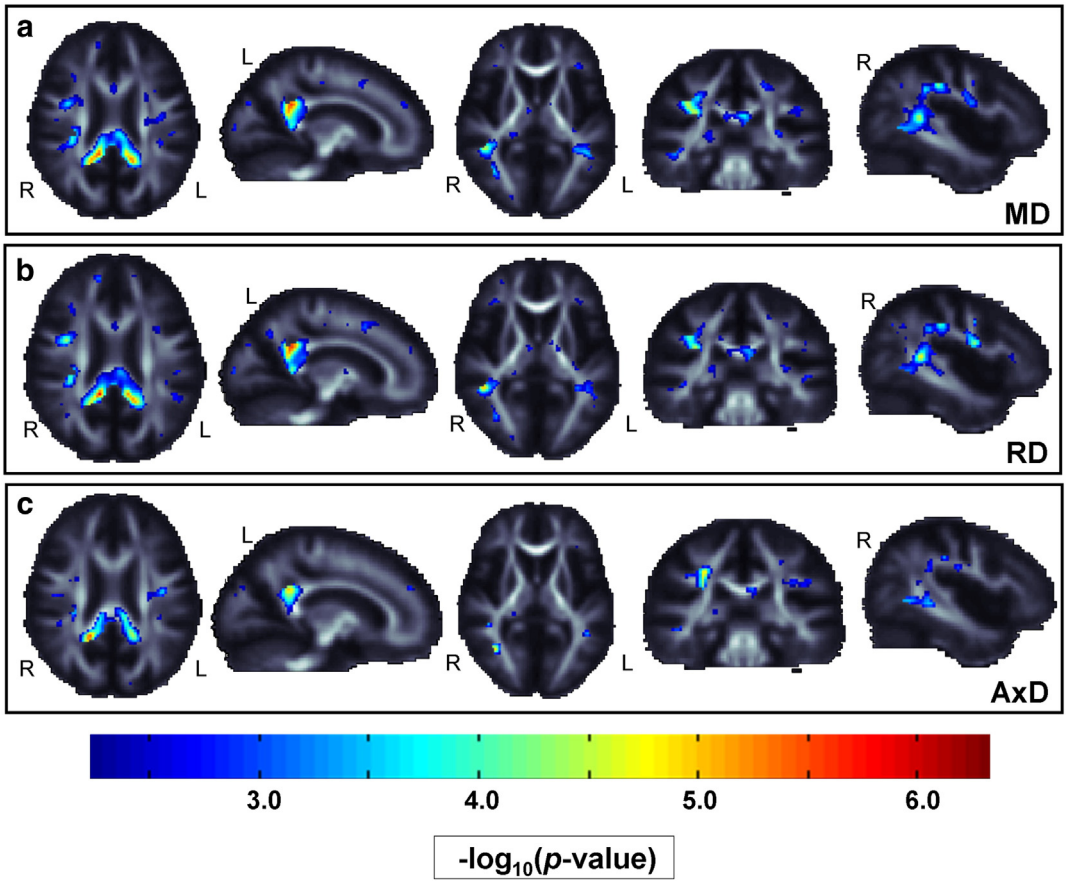

Fig. 5. Statistical maps show where CDR-sob scores are significantly positively associated with diffusivity measures in the MCI group, considered on its own (n = 88). Higher diffusivity, indicative of greater WM deficits, is associated with greater CDR-sob scores indicative of greater impairment. We find the "most significant" association (i.e., strongest voxel-wise effect) in the splenium of the corpus callosum and the posterior cingulum.

fasciculus was in the top 10 in almost all full cohort diffusivity analyses. When it came to picking up subtle differences within the MCI group, CDR-sob scores were most widely correlated with diffusivity in both VBA and ROI analyses. Prior studies also suggest that CDR-sob is a more sensitive clinical assessment than ADAS-cog and MMSE, and it may better relate to measures of atrophy on anatomical MRI (Hua et al., 2009).

Post-hoc analyses were conducted to assess if there was any association between DTI summary measures and executive function (ADNI-EF) and memory (ADNI-MEM) scores. These analyses revealed some of the strongest associations in temporal lobe tracts that subserve a variety of functions known to deteriorate during aging, including the bilateral sagittal stratum, that carries parts of the inferior fronto-occipital fasciculus and inferior longitudinal fasciculus, the hippocampal cingulum as well as the cingulum. ADNI-EF associations were additionally found in the total ROI and superior longitudinal fasciculus, while ADNI-MEM was associated with DTI measures in the external capsule, inferior fronto-occipital fasciculus and uncinate fasciculus. These regional differences could shed light on the network of brain regions, connected via white matter fiber bundles, involved in each task. Prior DTI studies have linked similar regions to performance in executive function and memory (Kantarci et al., 2011; Sasson et al., 2013).

As patterns of differences were often diffuse across the VBA WM map, the total WM ROI was sometimes one of the 10 lowest *p*-values, but it was never the absolute best. Therefore assessing individual ROIs may offer slightly more power to detect changes than a global summary measure (Jahanshad et al., 2013). In general, the most significant ROIs were found mainly in the left hemisphere (for example, the left hippocampal part of the cingulum was in the top 10 ROIs in by far the most analyses), which has also been found in some prior MRI and DTI studies (Fox et al., 1996; Thompson et al., 2001; Scahill et al., 2002; Thompson et al., 2003; Muller et al., 2005). A supplementary analysis revealed no evidence of greater variability in ROI measures in the right hemisphere that may be causing the better performance of left hemisphere ROIs (see supplementary text). TBSS ROI results did not differ dramatically from the full average ROI results and left hippocampal cingulum was again 'top 10' in the most analyses; however, it was closely followed by the right hippocampal cingulum.

Aside from the total ROI and bilateral IFO, the ROIs that were consistently significant in at least two analyses (Fig. 6) corroborate a pattern of degeneration in the temporal lobe and posterior temporo-parietal circuitry found in many other DTI studies of MCI and AD (Head et al., 2004; Stahl et al., 2007; Chua et al., 2008; Stebbins and Murphy, 2009); these include limbic tracts in the parahippocampal white matter, posterior cingulum, fornix, and splenium of the CC, and have been linked to lower cognitive scores (Rose et al., 2000; Bozzali et al., 2002; Takahashi et al., 2002; Yoshiura et al., 2002; Fellgiebel et al., 2004; Fellgiebel et al., 2005; Duan et al., 2006; Medina et al., 2006; Rose et al., 2006; Zhang et al., 2007; Medina and Gaviria, 2008; Mielke et al., 2009). DTI studies have found lower anisotropy in the white matter pathway of the cingulate gyrus, particularly the posterior cingulum, which connects to the entorhinal cortex and plays a role in the cholinergic system, known to be impaired in AD (Perry, 1980; Selden et al., 1998; Takahashi et al., 2002; Medina et al., 2006; Zhang et al., 2007). In fact, it has been highly implicated in studies comparing MCI to controls, especially on the left as in our study (Fellgiebel et al., 2005; Medina et al., 2006; Rose et al., 2006; Zhang et al., 2007; Chua et al.,

Table 3
Atlas ROI average anisotropy and diffusivity. While many regions were statistically significant (Benjamini and Hochberg, 1995), here we highlight regions with the "top 10" significant *p*-values (greatest effect sizes) when comparing mean values between diagnostic groups (in the left column we show the diagnostic groups being compared). We also note the total number of significant ROIs (after FDR correction) out of the 43 tested and the critical FDR *p*-value.

	FA		MD		RD		AxD	
	ROI	*p*-value	ROI	*p*-value	ROI	*p*-value	ROI	*p*-value
a)	Fx/ST L	1.44E−7	SS L	2.09E−11	SS L	6.19E−11	SS L	6.29E−11
NC	SCC	1.40E−6	CGH L	1.23E−9	CGH L	1.69E−09	CGH L	1.68E−9
vs	TAP L	2.46E−6	TOTAL	4.63E−9	TOTAL	6.89E−09	TOTAL	7.47E−9
AD	PTR L	2.07E−5	SCR L	1.11E−8	SCR L	6.22E−08	SCR L	1.74E−8
	CC	4.41E−5	SCC	6.54E−8	PTR L	7.64E−08	IFO L	3.04E−8
	SFO R	5.86E−5	Fx/ST L	1.07E−7	Fx/ST L	7.70E−08	SS R	9.02E−8
	TAP R	8.79E−5	PTR L	1.10E−7	SCC	8.05E−08	Fx/ST L	2.54E−7
	ACR L	1.35E−4	SS R	1.24E−7	TAP L	1.25E−07	EC L	3.21E−7
	TOTAL	1.62E−4	TAP L	1.43E−7	ACR L	1.40E−07	SCC	3.34E−7
	CGH L	1.84E−4	IFO L	2.77E−7	SCR R	2.82E−07	UNC L	3.46E−7
# sig/43	24 ($p < 2.32E-2$)		42 ($p < 2.54E-2$)		42 ($p < 2.72E-2$)		41 ($p < 4.23E-2$)	
b)	–	–	CGH L	5.65E−5	CGH L	8.47E−5	CGH L	6.91E−5
NC	–	–	SCC	2.60E−3	SCC	3.23E−3	SS L	3.18E−3
vs	–	–	Fx/ST L	4.39E−3	Fx/ST L	3.89E−3	SCC	3.65E−3
MCI	–	–	TAP L	5.14E−3	TAP L	4.48E−3	Fx/ST L	6.06E−3
	–	–	SS L	5.48E−3	–	–	TOTAL	6.14E−3
	–	–	–	–	–	–	SS R	6.92E−3
	–	–	–	–	–	–	PTR L	7.20E−3
	–	–	–	–	–	–	SCR L	8.80E−3
	–	–	–	–	–	–	TAP L	8.86E−3
	–	–	–	–	–	–	EC R	1.01E−2
# sig/43	0		5 ($p < 5.47E-3$)		4 ($p < 4.48E-3$)		12 ($p < 1.23E-2$)	
c)	–	–	CGH L	6.16E−4	CGH L	7.33E−4	CGH L	8.92E−4
NC	–	–	SCR L	3.18E−3	–	–	–	–
vs	–	–	SCC	3.35E−3	–	–	–	–
e-MCI								
# sig/43	0		3 ($p < 3.35E-3$)		1 ($p < 7.33E-4$)		1 ($p < 8.92E-4$)	
d)	–	–	CGH L	4.71E−5	CGH L	9.53E−5	CGH L	3.01E−5
NC	–	–	–	–	–	–	SS L	1.88E−4
vs	–	–	–	–	–	–	SS R	1.47E−3
l-MCI	–	–	–	–	–	–	Fx/ST L	5.38E−3
	–	–	–	–	–	–	PTR L	5.68E−3
# sig/43	0		1 ($p < 4.71E-5$)		1 ($p < 9.53E-5$)		5 ($p < 5.678E-3$)	

2008). Cognitive scores like MMSE have also been linked to DTI diffusivity values in the posterior cingulate gyrus in AD (Yoshiura et al., 2002; Fellgiebel et al., 2005). Most AD studies also find WM deficits in the corpus callosum, but it is not clear whether the genu is more affected (Xie et al., 2006), in line with the hypothesis that later maturing regions are the first affected, or the splenium, corroborating a pattern of degeneration in the posterior temporal parietal circuitry (Takahashi et al., 2002; Medina et al., 2006; Duan et al., 2006). A review by Chua et al. (2008) reports that in healthy aging, DTI abnormalities occur in the frontal regions, specifically the frontal white matter, anterior cingulum and the genu of the corpus callosum, while in AD, DTI abnormalities are concentrated in the posterior regions. Some studies have dissociated the regional effects of age and dementia, with age effects greater in the anterior corpus callosum and frontal white matter, suggesting an anterior-to-posterior gradient, while individuals with early-stage dementia exhibit minimal additional frontal deficits, but rather show greater white matter deterioration in posterior lobar regions (Head et al., 2004).

As in prior studies of aging and AD (Sullivan et al., 2010; Acosta-Cabronero et al., 2010), FA was the *least* sensitive measure when comparing diagnostic groups and cognitive score associations in both ROI and VBA analyses (Fig. 2). A recent study found that FA measured using TBSS was more strongly associated with spectroscopic measurements than FA measured using voxel-wise averaging which is susceptible to partial-averaging artifacts (Wijtenburg et al., 2012). However, we found that TBSS ROI results were not substantially different from data computed from averaging diffusion indices in full ROIs (Inline Supplementary Fig. S2). A recent AD DTI review – based on 55 different studies – noted that MD values have more discriminative power than FA values and higher effect sizes for case–control differences in the frontal, parietal, occipital and temporal lobes (Clerx et al., 2012). To explain age related increases in MD without significant FA changes, Zhang et al. (2011) suggested that brain degeneration in aging may be caused, in part, by tissue damage due to processes such as focal ischemia. This may result in lower tissue density, increasing water diffusivity but maintaining underlying directional structure.

FA and MD are summary measures based on the ratio and mean of the eigenvalues respectively, but AxD may reflect axonal injury, and RD may reflect demyelination (Song et al., 2003; Song et al., 2005; Sun et al., 2006; Hofling et al., 2009). Here, when comparing NC to AD patients in both ROI and VBA analyses, RD was the most strongly associated with WM deficits (Fig. 2a–b), followed by MD. Increased RD in AD relative to controls, therefore, may reflect demyelination in AD. As in prior studies that reported AxD increases in normal aging and Alzheimer's disease (Fellgiebel et al., 2004; Sullivan et al., 2010; Acosta-Cabronero et al., 2010; Agosta et al., 2011), we also found higher AxD in MCI, AD, and associated with clinical impairment. In fact, we found slightly larger effect sizes for AxD when comparing CN and l-MCI subjects in the VBA analyses, and CN and MCI subjects in the full ROI analyses (Table 3b). Recent longitudinal and cross-sectional studies suggest that AxD might be more sensitive to detecting early changes, while RD becomes progressively better as disease progresses (O'Dwyer et al., 2011; Acosta-Cabronero et al., 2012). Ultimately, the

Table 4
Atlas ROI average anisotropy and diffusivity. Here we highlight regions with the 10 lowest FDR significant (Benjamini and Hochberg, 1995) *p*-values (greatest effect sizes) when assessing cognitive test score associations in the entire study population. We also note the total number of significant ROIs (after FDR correction) out of the 43 tested and the critical FDR *p*-value.

	FA		MD		RD		AxD	
	ROI	*p*-value	ROI	*p*-value	ROI	*p*-value	ROI	*p*-value
a) MMSE	Fx/ST L	3.14E−5	CGH L	8.01E−15	CGH L	1.96E−14	CGH L	1.96E−14
	PTR L	2.11E−4	CGC L	2.05E−8	SS L	5.86E−8	SS R	4.47E−8
	ACR L	2.13E−4	SS L	2.98E−8	CGC L	9.93E−8	SS L	6.95E−8
	ACR R	3.60E−4	ACR L	1.57E−7	ACR L	1.22E−7	TOTAL	1.23E−7
	TOTAL	5.95E−4	SS R	1.83E−7	TOTAL	5.06E−7	UNC L	1.67E−7
	SCC	6.18E−4	TOTAL	2.46E−7	ACR R	7.63E−7	CGC L	3.61E−7
	CC	7.59E−4	IFO L	3.99E−7	SS R	9.68E−7	EC L	4.56E−7
	CP R	1.27E−3	Fx/ST L	9.60E−7	IFO L	1.17E−6	Fx/ST L	6.33E−7
	CGH L	1.42E−3	ACR R	1.17E−6	Fx/ST L	1.28E−6	CGH R	1.42E−6
	BCC	1.46E−3	CGH R	1.32E−6	IFO R	1.91E−6	RLIC L	2.04E−6
# sig/43	24 ($p < 2.78E-2$)		43 ($p < 1.76E-2$)		43 ($p < 3.66E-2$)		42 ($p < 2.37E-2$)	
b) CDR-sob	SCC	1.02E−5	CGH L	2.21E−12	CGH L	2.34E−12	CGH L	1.47E−11
	CC	1.38E−5	IFO R	1.06E−9	IFO R	4.29E−9	SS L	4.52E−9
	PTR L	4.49E−5	SS L	2.96E−9	SS L	9.54E−9	SS R	9.72E−9
	GCC	8.80E−5	IFO L	6.57E−9	IFO L	1.98E−8	IFO R	1.36E−8
	TOTAL	9.75E−5	CGC L	9.75E−9	TOTAL	6.20E−8	TOTAL	3.48E−8
	BCC	1.09E−4	SS R	3.75E−8	CGC L	6.69E−8	IFO L	5.56E−8
	Fx/ST L	1.28E−4	TOTAL	3.80E−8	ACR L	1.10E−7	CGC L	9.34E−8
	TAP L	2.17E−4	ACR L	1.44E−7	SS R	2.16E−7	CC	2.57E−7
	CGH L	2.75E−4	CC	1.48E−7	CC	2.68E−7	PCR L	2.79E−7
	ACR L	4.61E−4	SCR L	2.23E−7	SCR L	4.76E−7	UNC L	4.09E−7
# sig/43	25 ($p < 2.71E-2$)		42 ($p < 3.59E-2$)		42 ($p < 2.83E-2$)		40 ($p < 4.22E-2$)	
c) ADAS-cog	CGH L	1.68E−4	CGH L	3.26E−12	CGH L	2.14E−12	CGH L	6.56E−11
	PTR L	4.28E−4	SS L	2.09E−10	SS L	5.39E−10	SS L	4.55E−10
	SCC	6.74E−4	SS R	3.16E−9	SS R	2.43E−8	SS R	6.36E−10
	Fx/ST L	8.57E−4	IFO R	1.91E−8	IFO R	1.09E−7	EC L	3.63E−8
	GCC	1.32E−3	IFO L	8.13E−8	IFO L	6.38E−7	IFO R	1.19E−7
	CC	1.71E−3	CGC L	1.24E−7	CGC L	7.75E−7	TOTAL	2.01E−7
	SFO R	1.74E−3	TOTAL	5.02E−7	TOTAL	1.30E−6	IFO L	2.99E−7
	ACR R	1.75E−3	EC L	2.49E−6	ACR R	3.45E−6	CGC L	6.08E−7
	PTR R	3.29E−3	CGC R	3.61E−6	PTR L	1.06E−5	UNC L	8.48E−7
	TAP L	3.35E−3	ACR R	5.54E−6	ACR L	1.36E−5	SLF L	9.20E−7
# sig/43	17 ($p < 1.8E-2$)		41 ($p < 3.62E-2$)		41 ($p < 4.70E-2$)		39 ($p < 3.80E-2$)	

positive relationships between AD and both AxD and RD may explain why FA, a function of the ratio of these measures, reveals the least differences (Acosta-Cabronero et al., 2010), and could not pick up more subtle deficits in MCI (Fig. 2b,c; Table 3b–d, Table 4).

In addition, a summary measure such as FA, derived from a simple tensor model, may not capture the complexity of white matter architecture. DTI has some limitations in gauging fiber integrity in regions with extensive fiber crossing and mixing. High angular diffusion imaging (HARDI) can better resolve white matter multi-fiber distribution than DTI single-tensor models (Leow et al., 2009; Zhan et al., 2009). More sophisticated measures, such as a modified version of FA calculated from the HARDI data "tensor distribution function" (TDF), can better characterize the anisotropy in regions of fiber crossings (Zhan et al., 2009), and may better reveal FA differences that are due to loss in fiber coherence rather than simply partial-volume effects.

Further limitations of this study include the small sample size from each of the 14 sites, and unequal distribution of cases across sites (see Inline Supplementary Table S1). Despite accounting for site effects using a random-effects regression model and grouping the data by acquisition site, some cross-site differences may be unaccounted for in

Table 5
Atlas ROI average anisotropy and diffusivity. Here we highlight regions with the "top 10" FDR significant (Benjamini and Hochberg, 1995) *p*-values (greatest effect sizes) when assessing cognitive test score associations within diagnostic subgroups. We also note the total number of significant ROIs (after FDR correction) out of the 43 tested and the critical FDR *p*-value.

	FA		MD		RD		AxD	
	ROI	*p*-value	ROI	*p*-value	ROI	*p*-value	ROI	*p*-value
MMSE MCI	–	–	CGH L	2.65E−6	CGH L	5.02E−6	CGH L	3.50E−6
# sig/43	0		1 ($p < 2.65E-6$)		1 ($p < 5.02E-6$)		1 ($p < 3.50E-6$)	
MMSE e-MCI	–	–	CGH L	9.37E−5	CGH L	1.52E−4	CGH L	1.03E−4
# sig/43	0		1 ($p < 9.37E-5$)		1 ($p < 1.52E-4$)		1 ($p < 1.03E-4$)	
CDR-sob	–	–	SLF R	4.15E−4	–	–	SLF R	6.94E−5
MCI	–	–	–	–	–	–	SLF L	2.98E−4
	–	–	–	–	–	–	PCR R	1.03E−3
	–	–	–	–	–	–	SCC	1.64E−3
	–	–	–	–	–	–	CGC L	3.46E−3
# sig/43	0		1 ($p < 4.15E-4$)		0		5 ($p < 3.46E-3$)	

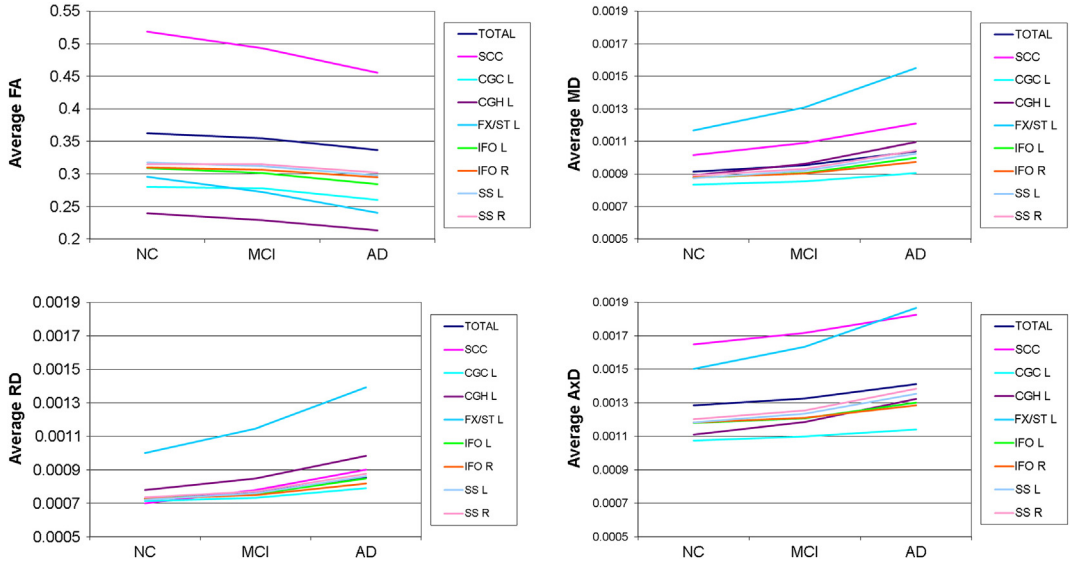

Fig. 6. Average FA and RD Y axis looks so much bigger than Average AxD and RD Y axis of the 43 ROIs, these 9 ROIs were consistently more sensitive to detecting differences across diffusivity and anisotropy measures in at least two cognitive and/or diagnostic analyses. These graphs show the average FA, MD, RD and AxD in the ROIs in each diagnostic group. "TOTAL" refers to the ROI generated by combining all the atlas ROIs. Overall, we see a decrease in anisotropy and increase in diffusivity with each stage of the disease.

the study design. Additionally we did not adjust for WMH burden, or explore the extent the DTI metrics corresponded with WMH. Finally, the ADNI data set is constantly re-evaluating subject diagnosis, cognitive, and basic demographic data. The data evaluated here was what was available at the time of download and may be modified by ADNI.

5. Conclusion

DTI offers an extensive set of biomarkers for disease detection and monitoring of cognitive decline. We found anisotropy and even more widespread diffusivity disruptions in projection, association, and commissural tracts, particularly in tracts that pass through the temporal lobe and posterior brain regions (especially the left hippocampal cingulum), in elderly AD and MCI patients. These disruptions were associated with neuropsychological and cognitive deficits. As ADNI2 progresses, new subjects are scanned and new measures of WMH are being added to the database. These results should be verified with larger sample sizes and the relationship between DTI based WM disturbances and WMH can be further resolved. Future tract-based connectivity studies may also shed light on how integrity in the tracts affects regional gray matter. We may also be able to create a statistical region-of-interest that may outperform atlas based ROIs (Hua et al., 2013; Gutman et al., 2013). ADNI2 is a longitudinal study that will eventually allow us to investigate which of these subjects develop AD, and if these early WM

Table 6
Cognitive correlates of the average anisotropy and diffusivity in different atlas regions of interest. Here we highlight regions with the "top 10" FDR significant (Benjamini and Hochberg, 1995) *p*-values (greatest effect sizes) when assessing executive function (ADNI-EF) and memory (ADNI-MEM) composite neuropsychological score associations in the entire study population. We also note the total number of significant ROIs (after FDR correction) out of the 43 tested and the critical FDR *p*-value.

	FA		MD		RD		AxD	
	ROI	*p*-value	ROI	*p*-value	ROI	*p*-value	ROI	*p*-value
a) ADNI-EF	SS L	5.77E−5	SS L	1.85E−9	SS L	9.15E−10	SS L	4.21E−8
	TOTAL	1.38E−4	SS R	8.12E−9	SS R	8.81E−9	SS R	4.78E−8
	GCC	2.46E−4	CGC L	4.68E−8	CGC L	1.39E−7	CGC L	1.55E−6
	SS R	3.42E−4	CGC R	3.10E−7	CGH L	3.29E−7	CGC R	1.75E−6
	PTR R	4.33E−4	CGH L	6.04E−7	CGC R	1.62E−6	RLIC L	2.17E−6
	ACR L	4.66E−4	RLIC L	1.46E−6	TOTAL	1.63E−6	TOTAL	4.02E−6
	CC	4.83E−4	TOTAL	1.61E−6	IFO R	7.14E−6	CGH L	5.08E−6
	Fx/ST L	7.55E−4	IFO R	3.31E−6	ACR L	9.49E−6	EC L	5.85E−6
	PTR L	7.90E−4	SLF L	4.27E−6	ACR R	1.08E−5	SCC	7.35E−6
	SCC	8.84E−4	EC L	8.76E−6	SLF L	1.85E−5	SLF L	1.21E−5
# sig/43	28 ($p < 2.39E-2$)		43 ($p < 3.24E-2$)		43 ($p < 3.27E-2$)		41 ($p < 3.49E-2$)	
b) ADNI-MEM	–	–	CGH L	1.38E−9	CGH L	1.68E−9	CGH L	5.28E−9
	–	–	SS L	4.70E−8	SS L	1.26E−7	SS L	7.59E−8
	–	–	CGC L	4.14E−7	IFO R	2.41E−6	CGC L	2.88E−7
	–	–	IFO R	5.05E−7	CGC L	4.24E−6	SS R	4.83E−7
	–	–	IFO L	1.03E−6	IFO L	8.30E−6	EC L	8.94E−7
	–	–	SS R	2.21E−6	SS R	9.67E−6	IFO R	1.40E−6
	–	–	CGC R	4.87E−6	CGC R	3.68E−5	IFO L	1.44E−6
	–	–	EC L	2.14E−5	EC L	2.22E−4	CGC R	3.15E−6
	–	–	CGH R	1.33E−4	CGH R	3.36E−4	UNC L	4.44E−5
	–	–	UNC L	1.65E−4	UNC L	3.69E−4	CGH R	5.00E−5
# sig/43	0		35 ($p < 3.06E-2$)		33 ($p < 3.35E-2$)		35 ($p < 3.51E-2$)	

aberrations help predict future deficits and conversion to AD. Future studies combining machine learning methods with different modalities – including CSF and proteomic markers – may ultimately determine the best way to distinguish diagnostic groups.

Acknowledgments

Data collection and sharing for this project was funded by ADNI (NIH Grant U01 AG024904). ADNI is funded by the National Institute on Aging, the National Institute of Biomedical Imaging and Bioengineering, and through generous contributions from the following: Abbott; Alzheimer's Association; Alzheimer's Drug Discovery Foundation; Amorfix Life Sciences Ltd.; AstraZeneca; Bayer HealthCare; BioClinica, Inc.; Biogen Idec Inc.; Bristol-Myers Squibb Company; Eisai Inc.; Elan Pharmaceuticals Inc.; Eli Lilly and Company; F. Hoffmann-La Roche Ltd. and its affiliated company Genentech, Inc.; GE Healthcare; Innogenetics, N.V.; IXICO Ltd.; Janssen Alzheimer Immunotherapy Research & Development, LLC.; Johnson & Johnson Pharmaceutical Research & Development LLC.; Medpace, Inc.; Merck & Co., Inc.; Meso Scale Diagnostics, LLC.; Novartis Pharmaceuticals Corporation; Pfizer Inc.; Servier; Synarc Inc.; and Takeda Pharmaceutical Company. The Canadian Institutes of Health Research is providing funds to support ADNI clinical sites in Canada. Private sector contributions are facilitated by the Foundation for the National Institutes of Health (www.fnih.org). The grantee organization is the Northern California Institute for Research and Education, and the study is coordinated by the Alzheimer's Disease Cooperative Study at the University of California, San Diego. ADNI data are disseminated by the Laboratory for Neuro Imaging at the University of California, Los Angeles. This research was also supported by NIH grants P30 AG010129 and K01 AG030514. Algorithm development for this study was also funded by the NIA, NIBIB, the National Library of Medicine, and the National Center for Research Resources (AG016570, EB01651, LM05639, RR019771 to PT). Investigators within ADNI contributed to the design and implementation of ADNI and/or provided data but did not participate in the analysis or writing of this report. For a complete listing of ADNI investigators, please see: http://adni.loni.ucla.edu/wp-content/uploads/how_to_apply/ADNI_Acknowledgement_List.pdf.

Appendix A. Supplementary data

Supplementary data to this article can be found online at http://dx.doi.org/10.1016/j.nicl.2013.07.006.

References

Acosta-Cabronero, J., Williams, G.B., Pengas, G., Nestor, P.J., 2010. Absolute diffusivities define the landscape of white matter degeneration in Alzheimer's disease. Brain 133 (Pt 2), 529–539.

Acosta-Cabronero, J., Alley, S., Williams, G.B., Pengas, G., Nestor, P.J., 2012. Diffusion tensor metrics as biomarkers in Alzheimer's disease. PLoS One 7 (11), e49072.

Agosta, F., Pievani, M., Sala, S., Geroldi, C., Galluzzi, S., Frisoni, G.B., Filippi, M., 2011. White matter damage in Alzheimer disease and its relationship to gray matter atrophy. Radiology 258 (3), 853–863.

Alzheimer's Disease Association, 2012. Alzheimer's disease facts and figures. Alzheimers Dement. 8 (2), 131–168.

Anderson, V.C., Litvack, Z.N., Kaye, J.A., 2005. Magnetic resonance approaches to brain aging and Alzheimer disease-associated neuropathology. Top. Magn. Reson. Imaging 16 (6), 439–452.

Apostolova, L.G., Thompson, P.M., 2008. Mapping progressive brain structural changes in early Alzheimer's disease and mild cognitive impairment. Neuropsychologia 46 (6), 1597–1612.

Apostolova, L.G., Mosconi, L., Thompson, P.M., Green, A.E., Hwang, K.S., Ramirez, A., Mistur, R., Tsui, W.H., de Leon, M.J., 2010. Subregional hippocampal atrophy predicts Alzheimer's dementia in the cognitively normal. Neurobiol. Aging 31 (7), 1077–1088.

Atiya, M., Hyman, B.T., Albert, M.S., Killiany, R., 2003. Structural magnetic resonance imaging in established and prodromal Alzheimer disease: a review. Alzheimer Dis. Assoc. Disord. 17 (3), 177–195.

Bakkour, A., Morris, J.C., Dickerson, B.C., 2009. The cortical signature of prodromal AD: regional thinning predicts mild AD dementia. Neurology 72 (12), 1048–1055.

Bartzokis, G., 2011. Alzheimer's disease as homeostatic responses to age-related myelin breakdown. Neurobiol. Aging 32 (8), 1341–1371.

Basser, P.J., Mattiello, J., LeBihan, D., 1994. MR diffusion tensor spectroscopy and imaging. Biophys. J. 66 (1), 259–267.

Benjamini, Y., Hochberg, Y., 1995. Controlling the false discovery rate — a practical and powerful approach to multiple testing. J. R. Stat. Soc. B Methodol. 57, 289–300.

Berg, L., 1988. Clinical Dementia Rating (CDR). Psychopharmacol. Bull. 24 (4), 637–639.

Bozzali, M., Falini, A., Franceschi, M., Cercignani, M., Zuffi, M., Scotti, G., Comi, G., Filippi, M., 2002. White matter damage in Alzheimer's disease assessed in vivo using diffusion tensor magnetic resonance imaging. J. Neurol. Neurosurg. Psychiatry 72 (6), 742–746.

Braak, H., Braak, E., 1991. Neuropathological stageing of Alzheimer-related changes. Acta Neuropathol. 82 (4), 239–259.

Braak, H., Braak, E., 1995. Staging of Alzheimer's disease-related neurofibrillary changes. Neurobiol. Aging 16 (3), 271–278.

Braak, H., Braak, E., 1996. Development of Alzheimer-related neurofibrillary changes in the neocortex inversely recapitulates cortical myelogenesis. Acta Neuropathol. 92 (2), 197–201.

Braskie, M.N., Jahanshad, N., Stein, J.L., Barysheva, M., McMahon, K.L., de Zubicaray, G.I., Martin, N.G., Wright, M.J., Ringman, J.M., Toga, A.W., Thompson, P.M., 2011. Common Alzheimer's disease risk variant within the CLU gene affects white matter microstructure in young adults. J. Neurosci. 31 (18), 6764–6770.

Brun, A., Englund, E., 1986. A white matter disorder in dementia of the Alzheimer type: a pathoanatomical study. Ann. Neurol. 19 (3), 253–262.

Bruscoli, M., Lovestone, S., 2004. Is MCI really just early dementia? A systematic review of conversion studies. Int. Psychogeriatr. 16 (2), 129–140.

Canu, E., McLaren, D.G., Fitzgerald, M.E., Bendlin, B.B., Zoccatelli, G., Alessandrini, F., Pizzini, F.B., Ricciardi, G.K., Beltramello, A., Johnson, S.C., Frisoni, G.B., 2010. Microstructural diffusion changes are independent of macrostructural volume loss in moderate to severe Alzheimer's disease. J. Alzheimers Dis. 19 (3), 963–976.

Capizzano, A.A., Acion, L., Bekinschtein, T., Furman, M., Gomila, H., Martinez, A., Mizrahi, R., Starkstein, S.E., 2004. White matter hyperintensities are significantly associated with cortical atrophy in Alzheimer's disease. J. Neurol. Neurosurg. Psychiatry 75 (6), 822–827.

Chetelat, G., Baron, J.C., 2003. Early diagnosis of Alzheimer's disease: contribution of structural neuroimaging. Neuroimage 18 (2), 525–541.

Chiang, G.C., Insel, P.S., Tosun, D., Schuff, N., Truran-Sacrey, D., Raptentsetsang, S., Jack Jr., C.R., Weiner, M.W., 2011. Identifying cognitively healthy elderly individuals with subsequent memory decline by using automated MR temporoparietal volumes. Radiology 259 (3), 844–851.

Chua, T.C., Wen, W., Slavin, M.J., Sachdev, P.S., 2008. Diffusion tensor imaging in mild cognitive impairment and Alzheimer's disease: a review. Curr. Opin. Neurol. 21 (1), 83–92.

Clerx, L., Visser, P.J., Verhey, F., Aalten, P., 2012. New MRI markers for Alzheimer's disease: a meta-analysis of diffusion tensor imaging and a comparison with medial temporal lobe measurements. J. Alzheimers Dis. 29 (2), 405–429.

Crane, P.K., Carle, A., Gibbons, L.E., Insel, P., Mackin, R.S., Gross, A., Jones, R.N., Mukherjee, S., Curtis, S.M., Harvey, D., Weiner, M., Mungas, D., 2012. Development and assessment of a composite score for memory in the Alzheimer's Disease Neuroimaging Initiative (ADNI). Brain Imaging Behav. 6 (4), 502–516.

Daianu, M., Jahanshad, N., Nir, T.M., Dennis, E., Toga, A.W., Jack, C.R., Weiner, M.W., Thompson, P.M., ADNI, 2012. Analyzing the structural k-core of brain connectivity networks in normal aging and Alzheimer's disease. MICCAI NIBAD, pp. 52–62.

Daianu, M., Dennis, E.L., Jahanshad, N., Nir, T.M., Toga, A.W., Jack, C.R., Weiner, M.W., Thompson, P.M., ADNI, 2013a. Alzheimer's disease disrupts rich club organization in brain connectivity networks. Proc. IEEE Int. Symp. Biomed. Imaging 266–269.

Daianu, M., Jahanshad, N., Nir, T.M., Toga, A.W., Jack, C.R., Weiner, M.W., Thompson, P.M., ADNI, 2013b. Breakdown of brain connectivity between normal aging and Alzheimer's disease: a structural k-core network analysis. Brain Connectivity 3 (4), 407–422.

de Leeuw, F.E., Barkhof, F., Scheltens, P., 2004. White matter lesions and hippocampal atrophy in Alzheimer's disease. Neurology 62 (2), 310–312.

Desikan, R.S., Cabral, H.J., Settecase, F., Hess, C.P., Dillon, W.P., Glastonbury, C.M., Weiner, M.W., Schmansky, N.J., Salat, D.H., Fischl, B., 2010a. Automated MRI measures predict progression to Alzheimer's disease. Neurobiol. Aging 31 (8), 1364–1374.

Desikan, R.S., Sabuncu, M.R., Schmansky, N.J., Reuter, M., Cabral, H.J., Hess, C.P., Weiner, M.W., Biffi, A., Anderson, C.D., Rosand, J., Salat, D.H., Kemper, T.L., Dale, A.M., Sperling, R.A., Fischl, B., 2010b. Selective disruption of the cerebral neocortex in Alzheimer's disease. PLoS One 5 (9), e12853.

Douaud, G., Jbabdi, S., Behrens, T.E., Menke, R.A., Gass, A., Monsch, A.U., Rao, A., Whitcher, B., Kindlmann, G., Matthews, P.M., Smith, S., 2011. DTI measures in crossing-fibre areas: increased diffusion anisotropy reveals early white matter alteration in MCI and mild Alzheimer's disease. Neuroimage 55 (3), 880–890.

Duan, J.H., Wang, H.Q., Xu, J., Lin, X., Chen, S.Q., Kang, Z., Yao, Z.B., 2006. White matter damage of patients with Alzheimer's disease correlated with the decreased cognitive function. Surg. Radiol. Anat. 28 (2), 150–156.

Fellgiebel, A., Wille, P., Muller, M.J., Winterer, G., Scheurich, A., Vucurevic, G., Schmidt, L.G., Stoeter, P., 2004. Ultrastructural hippocampal and white matter alterations in mild cognitive impairment: a diffusion tensor imaging study. Dement. Geriatr. Cogn. Disord. 18 (1), 101–108.

Fellgiebel, A., Muller, M.J., Wille, P., Dellani, P.R., Scheurich, A., Schmidt, L.G., Stoeter, P., 2005. Color-coded diffusion-tensor-imaging of posterior cingulate fiber tracts in mild cognitive impairment. Neurobiol. Aging 26 (8), 1193–1198.

Fischl, B., van der Kouwe, A., Destrieux, C., Halgren, E., Segonne, F., Salat, D.H., Busa, E., Seidman, L.J., Goldstein, J., Kennedy, D., Caviness, V., Makris, N., Rosen, B., Dale, A.M., 2004. Automatically parcellating the human cerebral cortex. Cereb. Cortex 14 (1), 11–22.

Folstein, M.F., Folstein, S.E., McHugh, P.R., 1975. "Mini-mental state". A practical method for grading the cognitive state of patients for the clinician. J. Psychiatr. Res. 12 (3), 189–198.
Fox, N.C., Warrington, E.K., Freeborough, P.A., Hartikainen, P., Kennedy, A.M., Stevens, J.M., Rossor, M.N., 1996. Presymptomatic hippocampal atrophy in Alzheimer's disease. A longitudinal MRI study. Brain 119 (Pt 6), 2001–2007.
Gibbons, L.E., Carle, A.C., Mackin, R.S., Harvey, D., Mukherjee, S., Insel, P., Curtis, S.M., Mungas, D., Crane, P.K., 2012. A composite score for executive functioning, validated in Alzheimer's Disease Neuroimaging Initiative (ADNI) participants with baseline mild cognitive impairment. Brain Imaging Behav. 6 (4), 517–527.
Gutman, B., Svarer, C., Leow, A.D., Yanovsky, I., Toga, A.W., Thompson, P.M., 2012. Creating unbiased minimal deformation templates for brain volume registration. Proceedings of the Organization for Human Brain Mapping Annual Conference.
Gutman, B.A., Hua, X., Rajagopalan, P., Chou, Y.Y., Wang, Y., Yanovsky, I., Toga, A.W., Jack Jr., C.R., Weiner, M.W., Thompson, P.M., 2013. Maximizing power to track Alzheimer's disease and MCI progression by LDA-based weighting of longitudinal ventricular surface features. Neuroimage 70, 386–401.
Guzman, V.A., Carmichael, O.T., Schwarz, C., Tosto, G., Zimmerman, M.E., Brickman, A.M., 2013. White matter hyperintensities and amyloid are independently associated with entorhinal cortex volume among individuals with mild cognitive impairment. Alzheimers Dement. http://dx.doi.org/10.1016/j.jalz.2012.11.009 (in press, Epub ahead of print).
Head, D., Buckner, R.L., Shimony, J.S., Williams, L.E., Akbudak, E., Conturo, T.E., McAvoy, M., Morris, J.C., Snyder, A.Z., 2004. Differential vulnerability of anterior white matter in nondemented aging with minimal acceleration in dementia of the Alzheimer type: evidence from diffusion tensor imaging. Cereb. Cortex 14 (4), 410–423.
Hebert, L.E., Scherr, P.A., Bienias, J.L., Bennett, D.A., Evans, D.A., 2003. Alzheimer disease in the US population: prevalence estimates using the 2000 census. Arch. Neurol. 60 (8), 1119–1122.
Hofling, A.A., Kim, J.H., Fantz, C.R., Sands, M.S., Song, S.K., 2009. Diffusion tensor imaging detects axonal injury and demyelination in the spinal cord and cranial nerves of a murine model of globoid cell leukodystrophy. NMR Biomed. 22 (10), 1100–1106.
Holmes, C.J., Hoge, R., Collins, L., Woods, R., Toga, A.W., Evans, A.C., 1998. Enhancement of MR images using registration for signal averaging. J. Comput. Assist. Tomogr. 22, 324–333.
Hua, X., Leow, A.D., Lee, S., Klunder, A.D., Toga, A.W., Lepore, N., Chou, Y.Y., Brun, C., Chiang, M.C., Barysheva, M., Jack Jr., C.R., Bernstein, M.A., Britson, P.J., Ward, C.P., Whitwell, J.L., Borowski, B., Fleisher, A.S., Fox, N.C., Boyes, R.G., Barnes, J., Harvey, D., Kornak, J., Schuff, N., Boreta, L., Alexander, G.E., Weiner, M.W., Thompson, P.M., ADNI, 2008. 3D characterization of brain atrophy in Alzheimer's disease and mild cognitive impairment using tensor-based morphometry. Neuroimage 41 (1), 19–34.
Hua, X., Lee, S., Yanovsky, I., Leow, A.D., Chou, Y.Y., Ho, A.J., Gutman, B., Toga, A.W., Jack Jr., C.R., Bernstein, M.A., Reiman, E.M., Harvey, D.J., Kornak, J., Schuff, N., Alexander, G.E., Weiner, M.W., Thompson, P.M., 2009. Optimizing power to track brain degeneration in Alzheimer's disease and mild cognitive impairment with tensor-based morphometry: an ADNI study of 515 subjects. Neuroimage 48 (4), 668–681.
Hua, X., Lee, S., Hibar, D.P., Yanovsky, I., Leow, A.D., Toga, A.W., Jack Jr., C.R., Bernstein, M.A., Reiman, E.M., Harvey, D.J., Kornak, J., Schuff, N., Alexander, G.E., Weiner, M.W., Thompson, P.M., 2010. Mapping Alzheimer's disease progression in 1309 MRI scans: power estimates for different inter-scan intervals. Neuroimage 51 (1), 63–75.
Hua, X., Hibar, D.P., Ching, C.R., Boyle, C.P., Rajagopalan, P., Gutman, B.A., Leow, A.D., Toga, A.W., Jack Jr., C.R., Harvey, D., Weiner, M.W., Thompson, P.M., 2013. Unbiased tensor-based morphometry: improved robustness and sample size estimates for Alzheimer's disease clinical trials. Neuroimage 66, 648–661.
Hugenschmidt, C.E., Peiffer, A.M., Kraft, R.A., Casanova, R., Deibler, A.R., Burdette, J.H., Maldjian, J.A., Laurienti, P.J., 2008. Relating imaging indices of white matter integrity and volume in healthy older adults. Cereb. Cortex 18 (2), 433–442.
Iglesias, J.E., Liu, C.Y., Thompson, P.M., Tu, Z., 2011. Robust brain extraction across datasets and comparison with publicly available methods. IEEE Trans. Med. Imaging 30 (9), 1617–1634.
Jack Jr., C.R., Bernstein, M.A., Borowski, B.J., Gunter, J.L., Fox, N.C., Thompson, P.M., Schuff, N., Krueger, G., Killiany, R.J., Decarli, C.S., Dale, A.M., Carmichael, O.W., Tosun, D., Weiner, M.W., 2010. Update on the magnetic resonance imaging core of the Alzheimer's Disease Neuroimaging Initiative. Alzheimers Dement. 6 (3), 212–220.
Jahanshad, N., Zhan, L., Bernstein, M.A., Borowski, B.J., Jack, C.R., Toga, A.W., Thompson, P.M., 2010a. Diffusion tensor imaging in seven minutes: determining trade-offs between spatial and directional resolution. Proc. IEEE Int. Symp. Biomed. Imaging 1161–1164.
Jahanshad, N., Lee, A.D., Barysheva, M., McMahon, K.L., de Zubicaray, G.I., Martin, N.G., Wright, M.J., Toga, A.W., Thompson, P.M., 2010b. Genetic influences on brain asymmetry: a DTI study of 374 twins and siblings. Neuroimage 52 (2), 455–469.
Jahanshad, N., Kochunov, P.V., Sprooten, E., Mandl, R.C., Nichols, T.E., Almasy, L., Blangero, J., Brouwer, R.M., Curran, J.E., de Zubicaray, G.I., Duggirala, R., Fox, P.T., Hong, L.E., Landman, B.A., Martin, N.G., McMahon, K.L., Medland, S.E., Mitchell, B.D., Olvera, R.L., Peterson, C.P., Starr, J.M., Sussmann, J.E., Toga, A.W., Wardlaw, J.M., Wright, M.J., Hulshoff Pol, H.E., Bastin, M.E., McIntosh, A.M., Deary, I.J., Thompson, P.M., Glahn, D.C., 2013. Multi-site genetic analysis of diffusion images and voxelwise heritability analysis: A pilot project of the ENIGMA-DTI working group. Neuroimage 81, 455–469.
Jenkinson, M., Bannister, P., Brady, M., Smith, S., 2002. Improved optimization for the robust and accurate linear registration and motion correction of brain images. Neuroimage 17 (2), 825–841.
Kantarci, K., Jack Jr., C.R., Xu, Y.C., Campeau, N.G., O'Brien, P.C., Smith, G.E., Ivnik, R.J., Boeve, B.F., Kokmen, E., Tangalos, E.G., Petersen, R.C., 2001. Mild cognitive impairment and Alzheimer disease: regional diffusivity of water. Radiology 219 (1), 101–107.
Kantarci, K., Senjem, M.L., Avula, R., Zhang, B., Samikoglu, A.R., Weigand, S.D., Przybelski, S.A., Edmonson, H.A., Vemuri, P., Knopman, D.S., Boeve, B.F., Ivnik, R.J., Smith, G.E., Petersen, R.C., Jack, C.R., 2011. Diffusion tensor imaging and cognitive function in older adults with no dementia. Neurology 77 (1), 26–34.
Kavcic, V., Ni, H., Zhu, T., Zhong, J., Duffy, C.J., 2008. White matter integrity linked to functional impairments in aging and early Alzheimer's disease. Alzheimers Dement. 4 (6), 381–389.
Kochunov, P., Glahn, D.C., Lancaster, J., Winkler, A., Karlsgodt, K., Olvera, R.L., Curran, J.E., Carless, M.A., Dyer, T.D., Almasy, L., Duggirala, R., Fox, P.T., Blangero, J., 2011. Blood pressure and cerebral white matter share common genetic factors in Mexican Americans. Hypertension 57 (2), 330–335.
Lee, J.E., Chung, M.K., Lazar, M., DuBray, M.B., Kim, J., Bigler, E.D., Lainhart, J.E., Alexander, A.L., 2009. A study of diffusion tensor imaging by tissue-specific, smoothing-compensated voxel-based analysis. Neuroimage 44 (3), 870–883.
Leow, A.D., Yanovsky, I., Chiang, M.C., Lee, A.D., Klunder, A.D., Lu, A., Becker, J.T., Davis, S.W., Toga, A.W., Thompson, P.M., 2007. Statistical properties of Jacobian maps and the realization of unbiased large-deformation nonlinear image registration. IEEE Trans. Med. Imaging 26 (6), 822–832.
Leow, A.D., Zhu, S., Zhan, L., McMahon, K., de Zubicaray, G.I., Meredith, M., Wright, M.J., Toga, A.W., Thompson, P.M., 2009. The tensor distribution function. Magn. Reson. Med. 61 (1), 205–214.
Lepore, N., Brun, C., Pennec, X., Chou, Y.Y., Lopez, O.L., Aizenstein, H.J., Becker, J.T., Toga, A.W., Thompson, P.M., 2007. Mean template for tensor-based morphometry using deformation tensors. Med. Image Comput. Comput. Assist. Interv. 10 (Pt 2), 826–833.
Leung, K.K., Bartlett, J.W., Barnes, J., Manning, E.N., Ourselin, S., Fox, N.C., 2013. Cerebral atrophy in mild cognitive impairment and Alzheimer disease: Rates and acceleration. Neurology 80 (7), 648–654.
Liu, Y., Spulber, G., Lehtimaki, K.K., Kononen, M., Hallikainen, I., Grohn, H., Kivipelto, M., Hallikainen, M., Vanninen, R., Soininen, H., 2011. Diffusion tensor imaging and tract-based spatial statistics in Alzheimer's disease and mild cognitive impairment. Neurobiol. Aging 32 (9), 1558–1571.
Medina, D., DeToledo-Morrell, L., Urresta, F., Gabrieli, J.D., Moseley, M., Fleischman, D., Bennett, D.A., Leurgans, S., Turner, D.A., Stebbins, G.T., 2006. White matter changes in mild cognitive impairment and AD: a diffusion tensor imaging study. Neurobiol. Aging 27 (5), 663–672.
Medina, D.A., Gaviria, M., 2008. Diffusion tensor imaging investigations in Alzheimer's disease: the resurgence of white matter compromise in the cortical dysfunction of the aging brain. Neuropsychiatr Dis Treat 4 (4), 737–742.
Mielke, M.M., Kozauer, N.A., Chan, K.C., George, M., Toroney, J., Zerrate, M., Bandeen-Roche, K., Wang, M.C., Vanzijl, P., Pekar, J.J., Mori, S., Lyketsos, C.G., Albert, M., 2009. Regionally-specific diffusion tensor imaging in mild cognitive impairment and Alzheimer's disease. Neuroimage 46 (1), 47–55.
Migliaccio, R., Agosta, F., Possin, K.L., Rabinovici, G.D., Miller, B.L., Gorno-Tempini, M.L., 2012. White matter atrophy in Alzheimer's disease variants. Alzheimers Dement. 8 (Suppl. 5), S78–S87 (e71–72).
Mohs, R.C., Rosen, W.G., Davis, K.L., 1983. The Alzheimer's disease assessment scale: an instrument for assessing treatment efficacy. Psychopharmacol. Bull. 19 (3), 448–450.
Mori, S., Oishi, K., Jiang, H., Jiang, L., Li, X., Akhter, K., Hua, K., Faria, A.V., Mahmood, A., Woods, R., Toga, A.W., Pike, G.B., Neto, P.R., Evans, A., Zhang, J., Huang, H., Miller, M.I., van Zijl, P., Mazziotta, J., 2008. Stereotaxic white matter atlas based on diffusion tensor imaging in an ICBM template. Neuroimage 40 (2), 570–582.
Muller, M.J., Greverus, D., Dellani, P.R., Weibrich, C., Wille, P.R., Scheurich, A., Stoeter, P., Fellgiebel, A., 2005. Functional implications of hippocampal volume and diffusivity in mild cognitive impairment. Neuroimage 28 (4), 1033–1042.
Nir, T.M., Jahanshad, N., Toga, A.W., Bernstein, M.A., Jack, C.R., Weiner, M.W., Thompson, P.M., ADNI, 2012. Connectivity network breakdown predicts imminent volumetric atrophy in early mild cognitive impairment. MBIA Lect. Notes Comput. Sci. 7509, 41–50.
O'Dwyer, L., Lamberton, F., Bokde, A.L., Ewers, M., Faluyi, Y.O., Tanner, C., Mazoyer, B., O'Neill, D., Bartley, M., Collins, D.R., Coughlan, T., Prvulovic, D., Hampel, H., 2011. Multiple indices of diffusion identifies white matter damage in mild cognitive impairment and Alzheimer's disease. PLoS One 6 (6), e21745.
Oishi, K., Faria, A., Jiang, H., Li, X., Akhter, K., Zhang, J., Hsu, J.T., Miller, M.I., van Zijl, P.C., Albert, M., Lyketsos, C.G., Woods, R., Toga, A.W., Pike, G.B., Rosa-Neto, P., Evans, A., Mazziotta, J., Mori, S., 2009. Atlas-based whole brain white matter analysis using large deformation diffeomorphic metric mapping: application to normal elderly and Alzheimer's disease participants. Neuroimage 46 (2), 486–499.
Oishi, K., Faria, A., van Zijl, P.C.M., Mori, S., 2011. MRI Atlas of Human White Matter, second edition. Elsevier, Amsterdam.
Perry, E.K., 1980. The cholinergic system in old age and Alzheimer's disease. Age Ageing 9 (1), 1–8.
Petersen, R.C., Doody, R., Kurz, A., Mohs, R.C., Morris, J.C., Rabins, P.V., Ritchie, K., Rossor, M., Thal, L., Winblad, B., 2001. Current concepts in mild cognitive impairment. Arch. Neurol. 58 (12), 1985–1992.
Prasad, G., Nir, T.M., Toga, A.W., Thompson, P.M., ADNI, 2013. Tractography density and network measures in Alzheimer's disease. Proc. IEEE Int. Symp. Biomed. Imaging 692–695.
Risacher, S.L., Saykin, A.J., West, J.D., Shen, L., Firpi, H.A., McDonald, B.C., 2009. Baseline MRI predictors of conversion from MCI to probable AD in the ADNI cohort. Curr. Alzheimer Res. 6 (4), 347–361.
Rohlfing, T., 2013. Incorrect ICBM-DTI-81 atlas orientation and white matter labels. Front. Neurosci. 7, 4.
Rose, S.E., Chen, F., Chalk, J.B., Zelaya, F.O., Strugnell, W.E., Benson, M., Semple, J., Doddrell, D.M., 2000. Loss of connectivity in Alzheimer's disease: an evaluation of white matter tract integrity with colour coded MR diffusion tensor imaging. J. Neurol. Neurosurg. Psychiatry 69 (4), 528–530.
Rose, S.E., McMahon, K.L., Janke, A.L., O'Dowd, B., de Zubicaray, G., Strudwick, M.W., Chalk, J.B., 2006. Diffusion indices on magnetic resonance imaging and neuropsychological

performance in amnestic mild cognitive impairment. J. Neurol. Neurosurg. Psychiatry 77 (10), 1122–1128.
Rosen, W.G., Mohs, R.C., Davis, K.L., 1984. A new rating scale for Alzheimer's disease. Am. J. Psychiatry 141 (11), 1356–1364.
Sasson, E., Doniger, G.M., Pasternak, O., Tarrasch, R., Assaf, Y., 2013. White matter correlates of cognitive domains in normal aging with diffusion tensor imaging. Front. Neurosci. 7.
Sattler, C., Toro, P., Schonknecht, P., Schroder, J., 2012. Cognitive activity, education and socioeconomic status as preventive factors for mild cognitive impairment and Alzheimer's disease. Psychiatry Res. 196 (1), 90–95.
Scahill, R.I., Schott, J.M., Stevens, J.M., Rossor, M.N., Fox, N.C., 2002. Mapping the evolution of regional atrophy in Alzheimer's disease: unbiased analysis of fluid-registered serial MRI. Proc. Natl. Acad. Sci. U. S. A. 99 (7), 4703–4707.
Selden, N.R., Gitelman, D.R., Salamon-Murayama, N., Parrish, T.B., Mesulam, M.M., 1998. Trajectories of cholinergic pathways within the cerebral hemispheres of the human brain. Brain 121 (Pt 12), 2249–2257.
Sjobeck, M., Haglund, M., Englund, E., 2005. Decreasing myelin density reflected increasing white matter pathology in Alzheimer's disease — a neuropathological study. Int. J. Geriatr. Psychiatry 20 (10), 919–926.
Smith, S.M., 2002. Fast robust automated brain extraction. Hum. Brain Mapp. 17 (3), 143–155.
Smith, S.M., Jenkinson, M., Johansen-Berg, H., Rueckert, D., Nichols, T.E., Mackay, C.E., Watkins, K.E., Ciccarelli, O., Cader, M.Z., Matthews, P.M., Behrens, T.E., 2006. Tract-based spatial statistics: voxelwise analysis of multi-subject diffusion data. Neuroimage 31 (4), 1487–1505.
Song, S.K., Sun, S.W., Ju, W.K., Lin, S.J., Cross, A.H., Neufeld, A.H., 2003. Diffusion tensor imaging detects and differentiates axon and myelin degeneration in mouse optic nerve after retinal ischemia. Neuroimage 20 (3), 1714–1722.
Song, S.K., Yoshino, J., Le, T.Q., Lin, S.J., Sun, S.W., Cross, A.H., Armstrong, R.C., 2005. Demyelination increases radial diffusivity in corpus callosum of mouse brain. Neuroimage 26 (1), 132–140.
Stahl, R., Dietrich, O., Teipel, S.J., Hampel, H., Reiser, M.F., Schoenberg, S.O., 2007. White matter damage in Alzheimer disease and mild cognitive impairment: assessment with diffusion-tensor MR imaging and parallel imaging techniques. Radiology 243 (2), 483–492.
Stebbins, G.T., Murphy, C.M., 2009. Diffusion tensor imaging in Alzheimer's disease and mild cognitive impairment. Behav. Neurol. 21 (1), 39–49.
Stricker, N.H., Schweinsburg, B.C., Delano-Wood, L., Wierenga, C.E., Bangen, K.J., Haaland, K.Y., Frank, L.R., Salmon, D.P., Bondi, M.W., 2009. Decreased white matter integrity in late-myelinating fiber pathways in Alzheimer's disease supports retrogenesis. Neuroimage 45 (1), 10–16.
Sullivan, E.V., Rohlfing, T., Pfefferbaum, A., 2010. Quantitative fiber tracking of lateral and interhemispheric white matter systems in normal aging: relations to timed performance. Neurobiol. Aging 31 (3), 464–481.
Sun, S.W., Liang, H.F., Trinkaus, K., Cross, A.H., Armstrong, R.C., Song, S.K., 2006. Noninvasive detection of cuprizone induced axonal damage and demyelination in the mouse corpus callosum. Magn. Reson. Med. 55 (2), 302–308.
Takahashi, S., Yonezawa, H., Takahashi, J., Kudo, M., Inoue, T., Tohgi, H., 2002. Selective reduction of diffusion anisotropy in white matter of Alzheimer disease brains measured by 3.0 Tesla magnetic resonance imaging. Neurosci. Lett. 332 (1), 45–48.
Thompson, P.M., Mega, M.S., Woods, R.P., Zoumalan, C.I., Lindshield, C.J., Blanton, R.E., Moussai, J., Holmes, C.J., Cummings, J.L., Toga, A.W., 2001. Cortical change in Alzheimer's disease detected with a disease-specific population-based brain atlas. Cereb. Cortex 11 (1), 1–16.
Thompson, P.M., Hayashi, K.M., de Zubicaray, G., Janke, A.L., Rose, S.E., Semple, J., Herman, D., Hong, M.S., Dittmer, S.S., Doddrell, D.M., Toga, A.W., 2003. Dynamics of gray matter loss in Alzheimer's disease. J. Neurosci. 23 (3), 994–1005.
Thompson, P.M., Hayashi, K.M., Dutton, R.A., Chiang, M.C., Leow, A.D., Sowell, E.R., De Zubicaray, G., Becker, J.T., Lopez, O.L., Aizenstein, H.J., Toga, A.W., 2007. Tracking Alzheimer's disease. Ann. N. Y. Acad. Sci. 1097, 183–214.
Toga, A.W., Thompson, P.M., 2013. Connectomics sheds new light on Alzheimer's disease. Biol. Psychiatry 73 (5), 390–392.
Ukmar, M., Makuc, E., Onor, M.L., Garbin, G., Trevisiol, M., Cova, M.A., 2008. Evaluation of white matter damage in patients with Alzheimer's disease and in patients with mild cognitive impairment by using diffusion tensor imaging. Radiol. Med. 113 (6), 915–922.
Wakana, S., Nagae-Poetscher, L.M., Jiang, H., van Zijl, P., Golay, X., Mori, S., 2005. Macroscopic orientation component analysis of brain white matter and thalamus based on diffusion tensor imaging. Magn. Reson. Med. 53 (3), 649–657.
Wechsler, D., 1987. WMS-R: Wechsler Memory Scale-Revised: Manual. Harcourt Brace Jovanovich.
Weiner, M.W., Veitch, D.P., Aisen, P.S., Beckett, L.A., Cairns, N.J., Green, R.C., Harvey, D., Jack, C.R., Jagust, W., Liu, E., Morris, J.C., Petersen, R.C., Saykin, A.J., Schmidt, M.E., Shaw, L., Siuciak, J.A., Soares, H., Toga, A.W., Trojanowski, J.Q., 2012. The Alzheimer's Disease Neuroimaging Initiative: a review of papers published since its inception. Alzheimers Dement. 8 (Suppl. 1), S1–S68.
Wijtenburg, S.A., McGuire, S.A., Rowland, L.M., Sherman, P.M., Lancaster, J.L., Tate, D.F., Hardies, L.J., Patel, B., Glahn, D.C., Hong, L.E., Fox, P.T., Kochunov, P., 2012. Relationship between fractional anisotropy of cerebral white matter and metabolite concentrations measured using (1)H magnetic resonance spectroscopy in healthy adults. Neuroimage 13, 161–168.
Xie, S., Xiao, J.X., Gong, G.L., Zang, Y.F., Wang, Y.H., Wu, H.K., Jiang, X.X., 2006. Voxel-based detection of white matter abnormalities in mild Alzheimer disease. Neurology 66 (12), 1845–1849.
Yanovsky, I., Thompson, P.M., Osher, S., Leow, A.D., 2007. Topology preserving log-unbiased nonlinear image registration: theory and implementation. IEEE Conf. Comput. Vis. Pattern Recognit. 1–8.
Yoshiura, T., Mihara, F., Ogomori, K., Tanaka, A., Kaneko, K., Masuda, K., 2002. Diffusion tensor in posterior cingulate gyrus: correlation with cognitive decline in Alzheimer's disease. Neuroreport 13 (17), 2299–2302.
Zhan, L., Chiang, M.C., Barysheva, M., Toga, A.W., McMahon, K.L., de Zubicaray, G.I., Meredith, M., Wright, M.J., Thompson, P.M., 2008. How many gradients are sufficient in high-angular resolution diffusion imaging (HARDI)? MICCAI CDMRI, pp. 216–224.
Zhan, L., Leow, A.D., Zhu, S., Baryshev, M., Toga, A.W., McMahon, K.L., de Zubicaray, G.I., Wright, M.J., Thompson, P.M., 2009. A novel measure of fractional anisotropy based on the tensor distribution function. Med. Image Comput. Comput. Assist. Interv. 12 (Pt 1), 845–852.
Zhan, L., Leow, A.D., Jahanshad, N., Chiang, M.C., Barysheva, M., Lee, A.D., Toga, A.W., McMahon, K.L., de Zubicaray, G.I., Wright, M.J., Thompson, P.M., 2010. How does angular resolution affect diffusion imaging measures? Neuroimage 49 (2), 1357–1371.
Zhan, L., Leow, A.D., Aganj, I., Lenglet, C., Sapiro, G., Yacoub, E., Harel, N., Toga, A.W., Thompson, P.M., 2011. Differential information content in staggered multiple shell HARDI measured by the tensor distribution function. Proc. IEEE Int. Symp. Biomed. Imaging 305–309.
Zhan, L., Jahanshad, N., Ennis, D.B., Jin, Y., Bernstein, M.A., Borowski, B.J., Jack Jr., C.R., Toga, A.W., Leow, A.D., Thompson, P.M., 2012. Angular versus spatial resolution trade-offs for diffusion imaging under time constraints. Hum. Brain Mapp. http://dx.doi.org/10.1002/hbm.2209 (in press, Epub ahead of print).
Zhan, L., Franc, D., Patel, V., Jahanshad, N., Jin, Y., Mueller, B.A., Bernstein, M.A., Borowski, B.J., Jack Jr., C.R., Toga, A.W., Lim, K.O., Thompson, P.M., 2012b. How do spatial and angular resolution affect brain connectivity maps from diffusion MRI? Proc. IEEE Int. Symp. Biomed. Imaging 1–6.
Zhang, Y., Schuff, N., Jahng, G.H., Bayne, W., Mori, S., Schad, L., Mueller, S., Du, A.T., Kramer, J.H., Yaffe, K., Chui, H., Jagust, W.J., Miller, B.L., Weiner, M.W., 2007. Diffusion tensor imaging of cingulum fibers in mild cognitive impairment and Alzheimer disease. Neurology 68 (1), 13–19.
Zhang, Y.Z., Chang, C., Wei, X.E., Fu, J.L., Li, W.B., 2011. Comparison of diffusion tensor image study in association fiber tracts among normal, amnestic mild cognitive impairment, and Alzheimer's patients. Neurol. India 59 (2), 168–173.